NATIONAL AERONAUTICS AND SPACE ADMINISTRATION

Technical Report 32-1479

Experimental Observations Relating the Inception of Liquid Rocket Engine Popping and Resonant Combustion to the Stagnation Dynamics of Injection Impingement

Richard M. Clayton

JET PROPULSION LABORATORY
CALIFORNIA INSTITUTE OF TECHNOLOGY
PASADENA, CALIFORNIA

December 15, 1970

NATIONAL AERONAUTICS AND SPACE ADMINISTRATION

Technical Report 32-1479

Experimental Observations Relating the Inception of Liquid Rocket Engine Popping and Resonant Combustion to the Stagnation Dynamics of Injection Impingement

Richard M. Clayton

JET PROPULSION LABORATORY
CALIFORNIA INSTITUTE OF TECHNOLOGY
PASADENA, CALIFORNIA

December 15, 1970

Preface

The work described in this report was performed by the Propulsion Division of the Jet Propulsion Laboratory.

Acknowledgment

The author gratefully acknowledges the outstanding support of John W. Short, who served as engineering test conductor for most of the engine experiments reported herein.

Contents

Contents (contd)

Tables

Figures

Contents (contd)

Figures (contd)

Abstract

Ordinary liquid rocket combustion processes are never truly steady processes. They are usually observed as low intensity, random combustion-chamber pressure variations. However, a clearly distinguishable, aperiodic form of nonsteadiness is also frequently observed. This form of nonsteadiness is characterized by discrete, large amplitude waves propagated throughout the combustion volume and is classified as popping. Popping and resonant combustion, as exhibited by annular and cylindrical versions of an 18-in.-diam engine, are found to occur for a particular range of propellant temperature and mixture ratio conditions used in a boundary (near wall) injection system.

The correlation of these conditions of temperature and mixture ratio is based on the argument that the impingement of two streams of equal dynamic pressure is inherently unsteady, and that small variations to either side of unity dynamic-pressure ratio can produce relatively large changes in the mixture and direction of the efflux from the impingement region. Pops are extremely effective in precipitating sustained combustion resonance unless the combustor is stabilized by control devices such as baffles. Reactive streams (hypergolic systems) and nonreactive streams (like-on-like systems) are discussed, as well as a proposed mechanism for producing initial combustion disturbances.

Experimental Observations Relating the Inception of Liquid Rocket Engine Popping and Resonant Combustion to the Stagnation Dynamics of Injection Impingement

I. Introduction

Liquid rocket combustion processes are never truly steady, and combustion noise is always generated, even in smoothly operating engines. Ordinary combustion noise, typically observed as low-intensity combustion-chamber pressure variations, is random in character; that is, a typical power spectral analysis conducted on a high-response chamber pressure measurement would reveal no predominant frequency of significant amplitude. Under these conditions, the time-average of the nonsteadiness can be considered to be equivalent to a steady condition for practical purposes (in much the same manner as is turbulent flow in a pipe).

Frequently, however, a form of nonsteadiness clearly distinguishable from ordinary noise is observed. It, too, is aperiodic, but is characterized by randomly occurring, large-amplitude, discrete pressure disturbances propagated as waves throughout the combustion volume. The occurrence of this phenomenon, as detected by high-response pressure measurements at the chamber boundaries, has been classified as *popping*. This phenomenon is most prominent with hypergolic propellants in combustion chambers of relatively large size (greater than several inches in diameter), which operate at moderate combustion pressures of a few hundred psi.

Operational engines in which popping has been identified or suspected during development include the *Titan/Gemini* launch engines, the *Apollo* service propulsion engine, and the *Transtage* engine (Refs. 1 and 2).

Pops are most often identified as disturbances that occur during otherwise steady operation; however, sharp disturbances that occur during starting transients are also often observed for both sea-level and vacuum starts. It is not clear whether the start-transient spikes are always initiated through the same mechanism that initiates the pops, but the result is generally the same—production of aperiodic, high-amplitude, steep-fronted traveling waves. Both of these spontaneously generated disturbances resemble the disturbance created initially by some engine-pulsing devices, such as those used in stability rating techniques. Indeed, the notion of *bombing* evidently arose as a consequence of the desire to test a given engine for its susceptibility to transition to resonant

(sustained periodic) combustion when exposed to such nonlinear waves. In any event, the potential of the spontaneously generated waves for precipitating combustion resonance is readily acknowledged, and an interest in understanding the origin and controlling process of these waves is well justified.

Various sources of pops have been proposed, and have been demonstrated for individual situations. Reference 2 outlines a mechanism involving the hydraulic flip phenomena associated with sharp-entry, short-tube-orifice configurations. In this type of configuration, a sudden change in the orifice flow properties perturbs the combustion processes as the flow either attaches or separates from the orifice bore near its exit. Reference 3 suggests propellant leaks from a defective injector as a source. More recently, evidence of *impingement-related* popping sources was observed in experiments on hypergolic stream-impingement phenomena (Refs. 4 and 5). Photographs in Refs. 4 and 5 showed the occurrence of intermittent violent disruptions of the impingement region under certain conditions. Although differing in detail, all of these candidate sources have in common the situation wherein a pulse of energy release has occurred locally.

It is not enough, however, that a small initial disturbance has occurred. Estimates (Ref. 6) based on spherical blast-wave theory indicate that a local energy release of the order of the total energy available in the chamber would be required if observed pops were always simply blast waves. In addition, as described below, observations indicate that wave strength is maintained (or sometimes increased) as the wave traverses the chamber —a characteristic that is the converse of the usual rapid decay of a blast wave with travel distance. Therefore, a more complete explanation of the pop disturbance involves combustion enhancement of initially small disturbances. Reference 6 presents an analysis of this enhancement with the use of a model introduced by Zel'dovich, Kogorko, and Simonov for the initiation of spherical detonation waves by blast waves. A principal conclusion drawn from the analysis is that spherical detonations might be initiated under reasonable rocket-combustion conditions with an initial energy release as small as 0.1% of the total chemical energy in the chamber. Furthermore, evidence that the liquid-rocket-combustion environment might support two-phase detonation processes is reported in Ref. 7.

Classical detonative phenomena during rocket combustion have rarely been verified experimentally (a task that is exceedingly difficult because the phenomena are superimposed on the steady combustion processes). However, considerable evidence exists that: (1) combustion enhancement of a relatively small initial disturbance can occur within the initial wave transit of reasonably large chambers, and (2) a high-amplitude wave would be manifested as a pop as it traverses or is reflected from the combustor boundaries.

During resonant-combustion experiments on several large research engines at JPL, two of the engines were observed to exhibit popping with exceptional persistence. Early attempts to isolate the cause of this rough combustion were not entirely successful, although certain operating variables were found to influence its occurrence (Refs. 8–10). Because it was believed that the more trivial sources of popping (i.e., anomalies such as leaky injectors and unstable streams) were absent in these engines, it was eventually suspected that the popping was related to impingement processes. Such processes have recently been studied in connection with so-called stream-separation phenomena (see Ref. 4 and Refs. 11–13), and have been shown to involve temperature and flow variables similar to those apparent in the present popping observations. When it was also considered that certain details of the fluid flow field resulting from the impingement of two free streams are dependent upon the relative dynamic pressures of the two streams, a correlation was obtained relating the occurrence of popping to the propellant temperature and dynamic pressure ratio of the boundary-injection scheme (Ref. 14).

This report presents the above correlation along with a more complete documentation of the supporting data from the aforementioned JPL experiments, together with additional recent results. Data are also presented that show details of the transient properties of the pressure wave associated with typical pop disturbances.

All of the results are from full-scale engine firings; therefore, from a fundamental standpoint, the experiments were of a relatively gross nature. Most of the data were obtained as a by-product of firings conducted with objectives other than the study of popping; hence, it is not purported that these results represent an exhaustive study of the subject. Rather, it is felt that the usefulness of this report is to document significant observations obtained on research engines reasonably representative of operational engines that also exhibit popping and resonance phenomena. These observations provide insight into injection-related aspects of the inception of non-

steady combustion, and the spontaneous transition from steady to resonant combustion, and should stimulate additional research on the fundamentals of stream-impingement processes. The results also provide a first-cut design criterion to improve the stability of liquid rocket engines.

II. Engine and Experimental Techniques

A. Engine

The 18-in.-diam engine used in these experiments is shown schematically in Fig. 1. Figure 2 shows the engine installed in the test stand in preparation for firing. Pertinent design conditions are listed in Table 1.

1. Cylindrical configuration. This assembly comprises an uncooled, heavy-walled combustion chamber/nozzle and an injector (designated RC-1). The injector is designed for N_2O_4–50/50(N_2H_4/UDMH) to produce a nominally uniform axial mass-flux of 0.31 lbm/s-in.^{2}; however, the total flow rate is divided (see Table 1) between main and boundary-injection systems. These two flows are separately manifolded and individually controlled by means of two feed systems on the test stand.

The unlike-doublet injector elements are arranged in seven concentric rows (see Fig. 1), and the mass-flux uniformity is achieved by having the flow from each concentric row of elements feed proportionately sized annular areas of the chamber cross section. For example, at design conditions, the boundary elements furnish 10% of the total flow to 10% of the chamber area. The geometry for both sets of elements (main and boundary) is shown in Fig. 1. This geometry satisfies the mixing-uniformity criterion (Ref. 15) at the design mixture ratios.

Table 1. Design conditions for 18-in.-diam cylindrical and annular engines using N_2O_4–50/50(N_2H_4/UDMH)

Parameter	Cylindrical configuration						Annular configuration					
	Boundary		Main		Overall		Boundary		Main		Overall	
	Fuel	Oxidizer	Fuel	Oxidizer	Fuel	Oxidizer	Fuel	Oxidizer	Fuel	Oxidizer	Fuel	Oxidizer
Flow rate, lbm/s	3.48	4.44	22.98	48.48	26.46	52.92	3.48	4.44	13.12	27.70	16.60	32.14
Injector Δp, psi (manifold to chamber)	108	96	129	120	—	—	108	96	129	120	—	—
Injection velocity V, ft/s	92	68	86	58	—	—	92	68	86	58	—	—
Element dynamic pressure ratio, p_{df}/p_{doz} $(=\rho_f V_f^2/\rho_{oz} V_{ox}^2)$	1.00		1.42		—		1.00		1.42		—	
Mixture ratio, m_{oz}/m_f	1.27		2.11		2.00		1.27		2.11		1.93	
Fraction of total flow	0.10[a]		0.90		1.00		0.163[a]		0.837		1.00	
Number of injector elements	24		84		108		24		48		72	
Characteristic length, in.	41.3						38.6					
Throat area, in.^{2}	127.7						79.3					
Engine contraction ratio	2.0						2.0					
Nozzle expansion ratio	1.29 or 2.95						1.46					
Thrust, lbf	14,500 or 14,700						9100					
Chamber pressure, psia	100						100					
Chamber mass flux, lbm/in.^{2}-s	0.31						0.31					

[a]Defined as Z.

(a) CUTAWAY VIEW OF ASSEMBLED INJECTOR

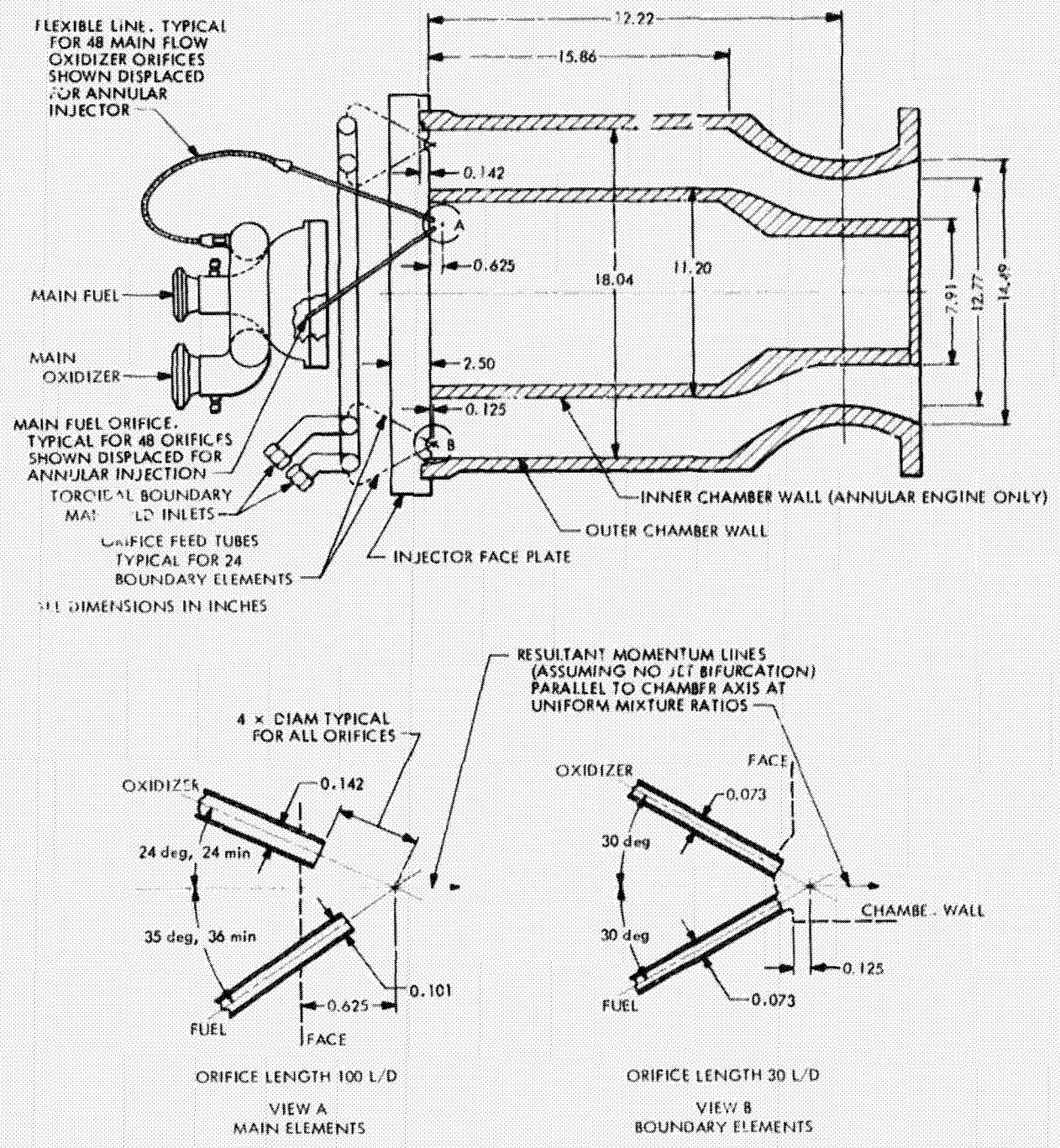

(b) FACE VIEW OF ASSEMBLED INJECTOR

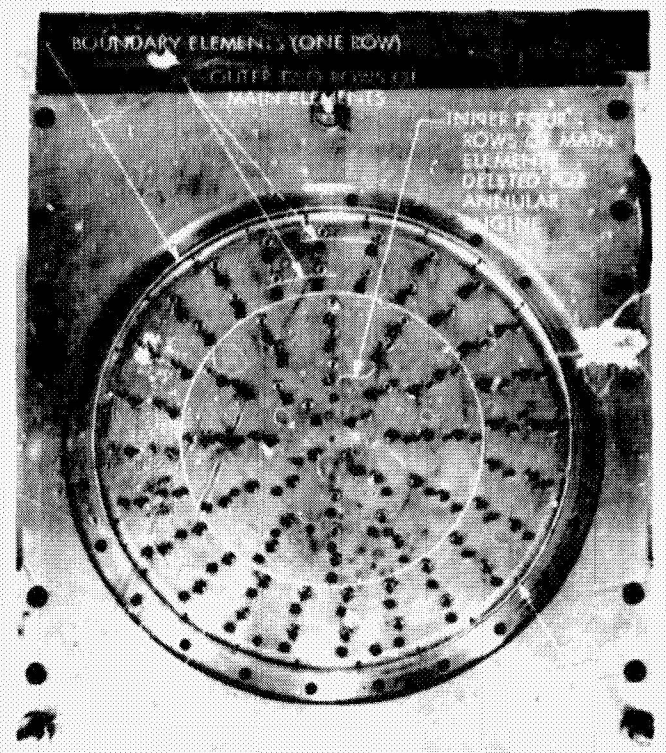

Fig. 1. Cylindrical and annular engine assemblies (18 in. diam)

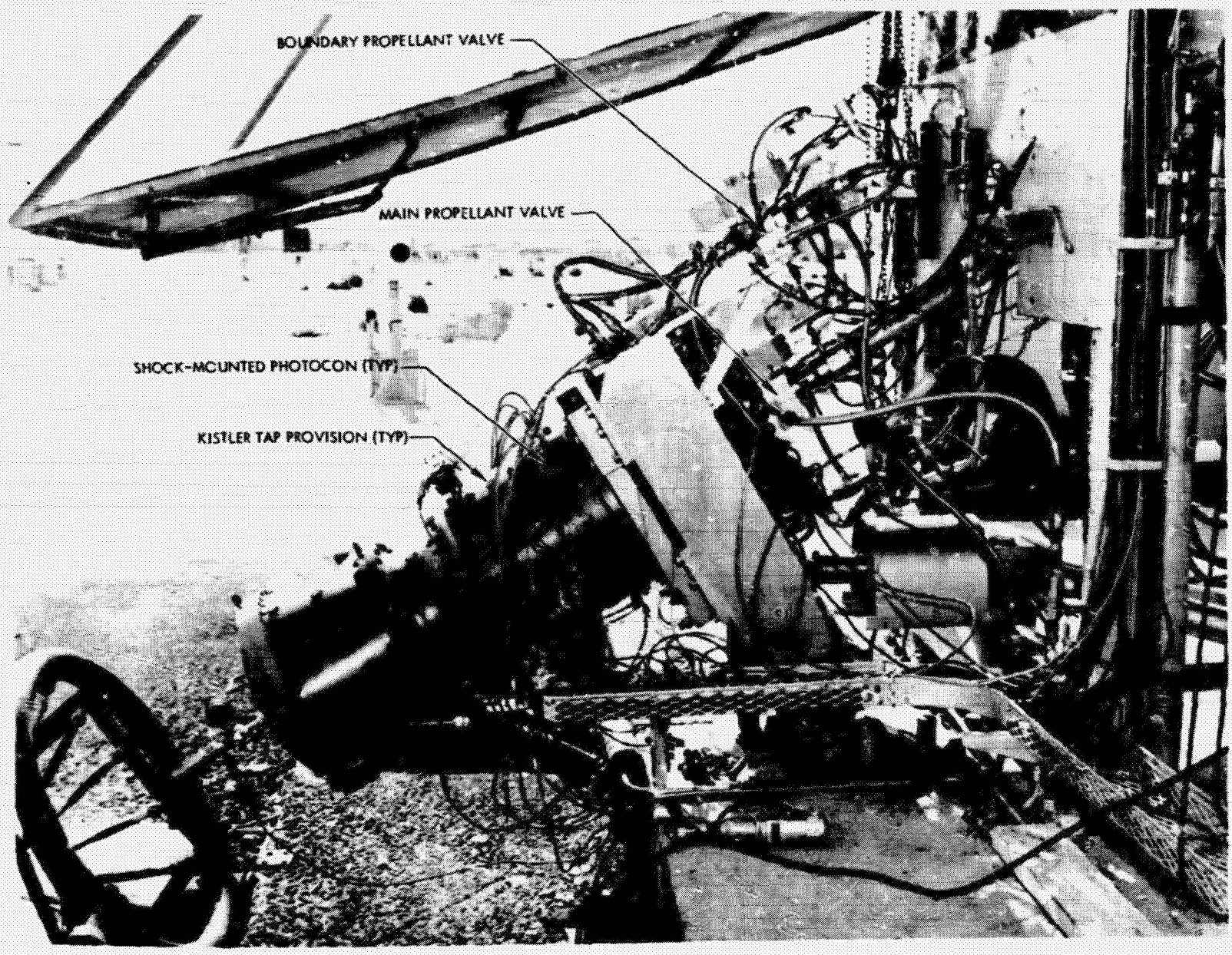

Fig. 2. Cylindrical engine mounted on test stand in preparation for firing

The design values for the main and boundary mixture ratios are not equal. The lower value for the boundary (1.27) is intended to provide relatively low-temperature reaction products adjacent to the chamber wall; however, the specific value of 1.27 was chosen so that equal-diameter boundary orifices could be used. As described in Ref. 8, this value, together with the separate feed systems, allowed alternate distributions of the injected propellants. The primary alternates that are referred to herein are:

(1) Bipropellant boundary flow, either oxidizer near-wall (design orientation) or fuel near-wall.

(2) Single-propellant boundary flow, either oxidizer or fuel (like impingement).

(3) Main flow only (boundary flow deleted).

(4) Boundary flow only (main flow deleted).

Figure 3a depicts the composite axial mass-distribution for the complete injector based on nonreactive spray data (see Ref. 15). Figures 3b and 3c depict the changes to the composite distribution for boundary-only and main-only flows, respectively.

As indicated in Fig. 1, the main and boundary orifices are fabricated from long, smooth-bore tubes (100 and 30 L/D, respectively). The turbulent flow and friction losses associated with these long orifices minimize maldistribution from the manifolds and attenuate coupling

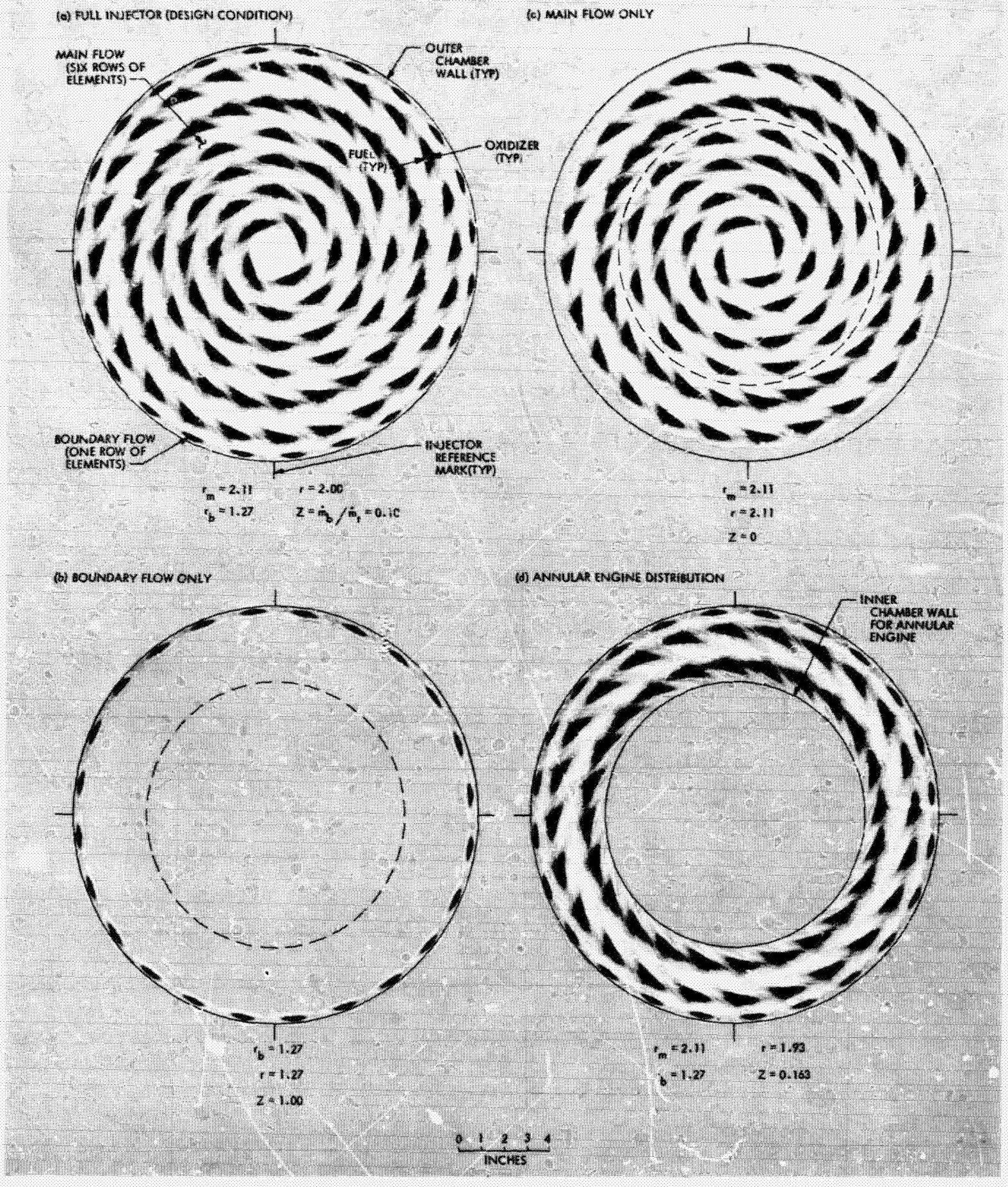

Fig. 3. Various axial mass-distributions used with the RC-1 injector 18-in.-diam cylindrical and annular engines; N_2O_4–50/50 fuel; nominal design flow conditions noted (all views looking upstream)

effects from nonsteady combustion-chamber pressure. Equally important is the fact that these orifices promote the control of the symmetry and reproducibility of the injected streams. Finally, the streams from these long orifices are free from any ordinary hydraulic flip effects; such effects are normally encountered only for short, sharp-edged orifices ($L/D < 10$).

When the cylindrical engine is baffled, the installation (Fig. 4) consists of an array of four blades of nearly radial orientation that are welded to the injector face and to a cylindrical centerpiece (the orifice arrangement is not altered). The blades are fabricated of aluminum sheet stock $\frac{3}{8}$ in. thick, and are carefully fitted so that no significant end gap (a few thousandths of an inch) exists at the outer chamber wall. The downstream edge of the baffle extends 2.9 in. beyond the injector face.

The steady-state performance of this engine is reported in Ref. 9. For design conditions, the engine yields a relative combustion performance of 97% (based on the ratio of measured c^* to theoretical equilibrium c^*). When the combustion is smooth and free of pops, the rms value of combustion noise is about 1 psi. (Reference 16 contains a discussion of this measurement.)

2. *Annular configuration.* The annular version of this engine is formed by inserting an 11.2-in.-diam centerbody into the cylindrical chamber and deleting the inner four rows of the original main injection elements, as shown in Figs. 1 and 3d. In this manner, an annular cavity with a width of 3.4 in. is formed. The cylindrical centerbody is bolted to the injector face, and extends along the engine axis to the nozzle. At the station of the nozzle entrance, the centerbody surface is contoured to

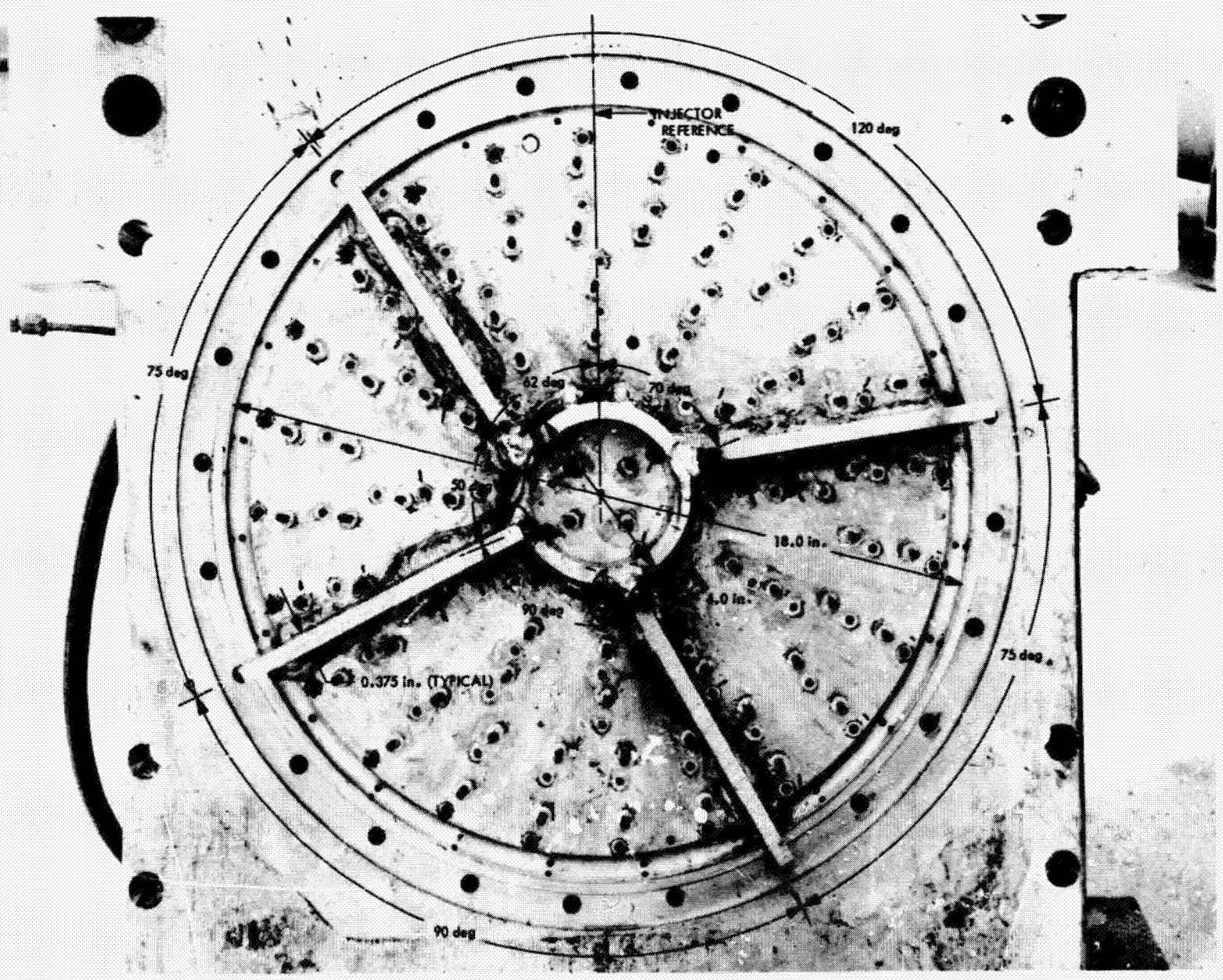

Fig. 4. Baffle installation, RC-1 injector

form the inner wall of the annular nozzle. The throat is maintained at its location for the cylindrical engine, and the nominal throat area is chosen to retain the cylindrical engine contraction ratio of 2.0:1. Figures 5 and 6 are views of the centerbody installation and the complete annular engine, respectively.

Deletion of flow from the four inner rows of main elements results in the annular injection distribution depicted in Fig. 3d, and (by virtue of the 11.2-in.-diam centerbody and the uniform mass-flux distribution of the RC-1 injector) the average mass flux $\bar{J}$ for the annular distribution is identical with the nominal flux for the full injector. Thus, the annular injector, designated RC-1 AN, presumably retains the same spatial distribution of the combustion processes (except for any effects caused by the presence of the inner wall).

Removable baffles are incorporated on the annular engine as shown in Fig. 5, and form an array of four 1-in.-thick blades, each bolted to the centerbody with a radial orientation and fitted to the mating centerbody and injector face surfaces. A layer of silastic rubber assures a seal at these interfaces. The outer ends of the aluminum blades are fitted as described for the cylindrical engine. The peripheral spacing is based on that used for the full engine, but the length of the blades is made variable by means of bolt-on extensions (not shown in Fig. 5). The length required to stabilize the annular engine was 2 in. greater than that for the cylindrical

Fig. 5. Centerbody installation, annular engine

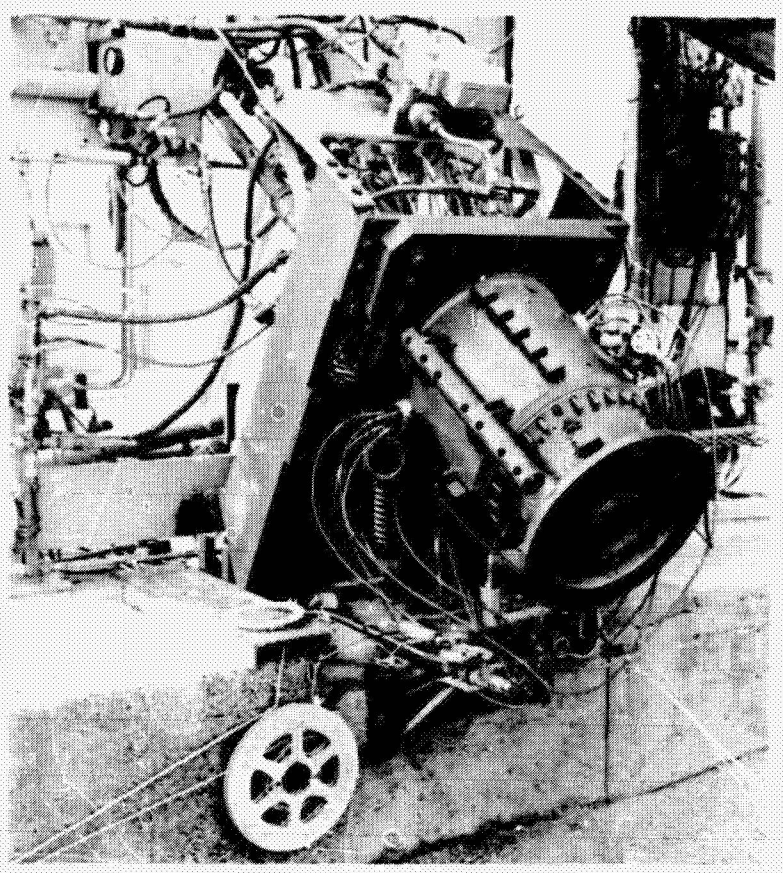

Fig. 6. Annular engine mounted on test stand in preparation for firing

version (see Ref. 10). Reference herein to inadequate baffles for the annular engine implies either that no baffles were used or that the baffles were less than 4.9 in. long.

At its design flow conditions, the annular engine yields a 93% relative combustion performance—a nominal reduction of 4% compared to the cylindrical engine. The lower performance is attributed to reduced secondary mixing of the main propellants because of the presence of the inner chamber wall (see Ref. 10). With the full injector, the arrangement of the main elements promotes a high degree of secondary mixing between adjacent rows of elements. For the annular engine, however, this source of mixing is curtailed for the innermost row of fuel streams because there is now an adjacent wall rather than adjacent oxidizer streams. This wall relationship can be seen in Fig. 3d. The inner row of elements furnishes 50% of the total main flow of propellants for the annular engine; therefore, degradation of propellant mixing in this region produces relatively large overall combustion performance losses. An improvement in performance of 1 to 2% was observed whenever pops increased the general turbulence level. Ordinary noise levels (when pops were absent) were 2 to 3 psi rms, or about double those of the cylindrical engine.

B. Propellant Feed Control

Propellants were supplied to the two portions of the injector from separate N_2 gas-pressurized run tanks through individual boundary and main propellant valves (see Fig. 2).

1. Flow. The significant features of the main valve and the start transient flow control (see Refs. 16 and 17) consist of controlling the starting flow by controlling the opening rate of the valve to approximate a monotonically increasing flow rate during the manifold fill and initial injection times with no flow overshoot. The fuel and oxidizer valve opening is sequenced to provide nominally simultaneous initial injection of the two propellants.

The aforementioned procedures produce a monotonic combustion-pressure transient except for occasional pressure spikes, which are usually the result of pressure-wave generation in the combustion chamber caused by discontinuous initial injection and combustion as the manifold ullage is purged by the incoming flow. The start spiking appeared to be more severe with higher propellant temperatures, which suggests that two-phase flow effects from N_2O_4 evaporation in the manifolds may have aggravated the spiking.

A smaller scale propellant valve, based on the same design as the main valve, is used to control the boundary flow starting transient. The boundary flow is generally commenced before the main flow so that it is near design conditions for 100 to 200 ms before main flow ignition.

2. Temperature. Propellant temperature was not originally considered to be an important variable influencing popping; therefore the main and boundary propellant temperatures were generally allowed to follow the ambient conditions at the test site.[1] Seasonal changes of climate resulted in propellant temperatures ranging from approximately 40 to 100°F.

For firings in which temperature-conditioned propellants were used, the propellants were conditioned to the desired temperature (~40 to 100°F) before transfer to the respective run tanks. Figure 7 shows one of the two temperature-conditioning units in position at the test stand.

C. Instrumentation

Steady-state measurements of chamber pressure, flow rates, thrust, injector manifold pressure, and propellant

[1]JPL Edwards Test Station, Edwards Air Force Base, Calif.

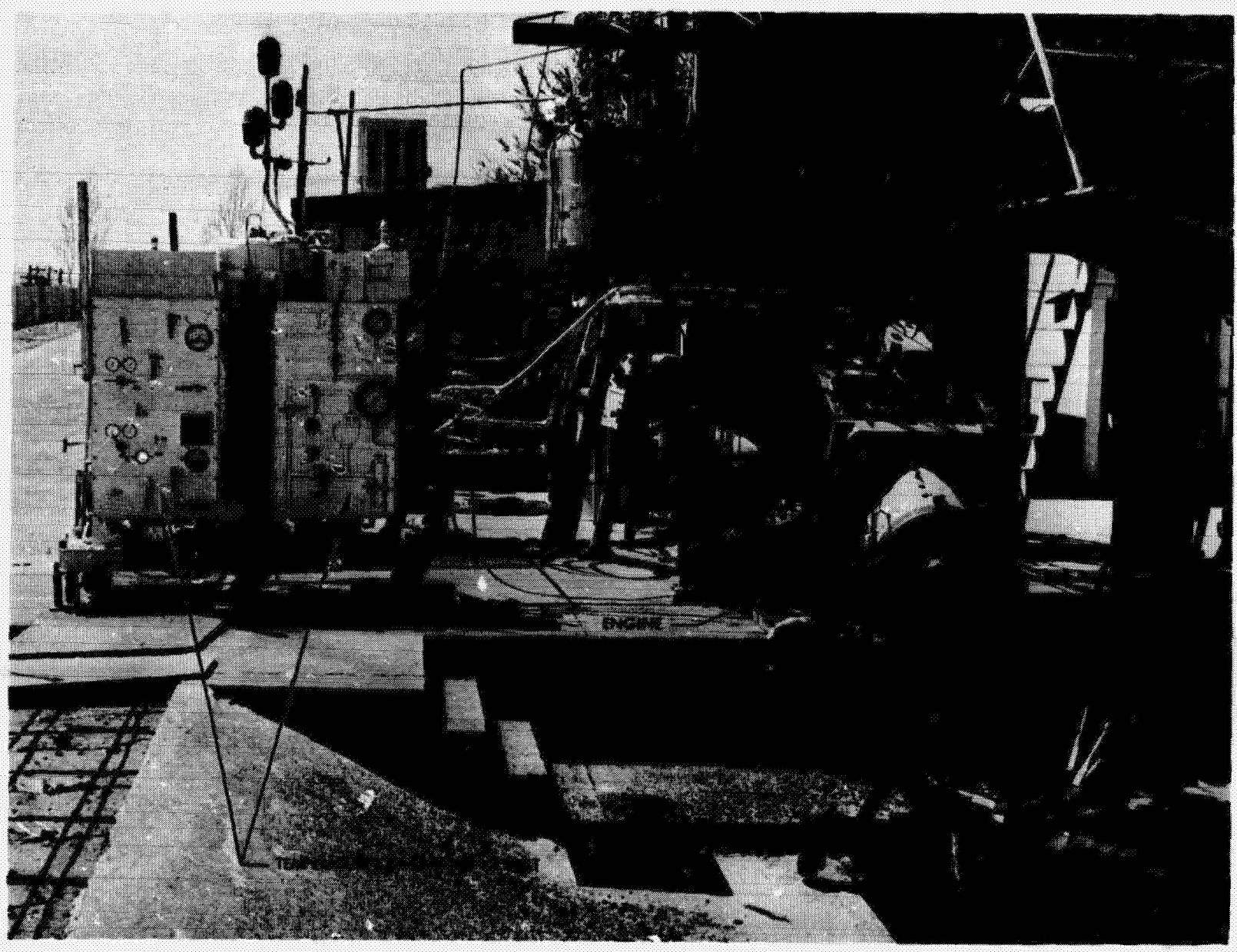

Fig. 7. Oxidizer temperature-conditioning unit in position at test stand

tank pressure were made for each firing. Typical measurement techniques used and the methods of performance computation are described in Ref. 16. Propellant temperature, flow rates, and high-response chamber pressure measurements are of particular interest for the data to be presented, and are discussed below.

1. Propellant temperature. All propellant temperatures were measured with thermocouple probes protruding into the respective fluid volumes. Thermocouple output signals were recorded digitally throughout each firing at approximate 17-ms intervals.

For those firings without temperature conditioning, the bulk propellant temperature in the tanks was measured, and was assumed to be equal to the injection temperature. This assumption is believed to be valid to within a few degrees because the initial injector hardware and fluid temperatures were nearly equal to the ambient air temperature for these short-duration tests.

For those runs with temperature conditioning, the propellant temperatures used for correlating popping data were measured at the respective manifolds.[2] As above, the manifold fluid temperature was recorded throughout the firing.

2. Flow rates. Main and boundary flows were measured individually with turbine flowmeters located in the

[2]The tanks and feed lines were not elaborately insulated; therefore, temperature gradients existed in the feed systems whenever the transferred propellant temperature differed greatly from the initial hardware temperature (nominally ambient air temperature). However, these gradients were considerably diminished during the approximately 30 min required between transfer and firing.

respective propellant feed lines. The output pulses from each flowmeter were continuously accumulated by a counter system, and the accumulated count was sampled and digitally recorded at intervals of 17 ms. Flows were calculated at each time interval (by computer) by the use of appropriate flowmeter calibration factors and propellant physical properties tables. Representative flow rates for each firing were taken as the average flow over 5 to 10 time intervals during the steady portion of the firing.

3. ***Chamber pressure transients.*** High-response chamber pressure measurements were made for all firings. At least one water-cooled Photocon (model 352 or 307) transducer channel (sometimes as many as four) was used for each firing. Provisions for these transducers were located on the face (one model 307) and on the outer chamber wall (three model 352s). The wall-mounted Photocons were soft-mounted to reduce mechanical vibration effects (Ref. 18). Provisions for an array of Kistler model 603A transducers located on the face and wall were also available for many of the firings. Again, the wall-mounted Kistler units were soft-mounted (see Ref. 18), whereas the face-mounted units were hard-mounted. All Kistler units were thermally protected by ablative techniques (see Ref. 18); therefore, their use was restricted to nominally 0.5-s firings. The locations of all of the high-response transducer taps are shown in Fig. 8. The outer chamber wall can be oriented circumferentially in increments of 3 deg relative to the injector reference mark, but Fig. 8 shows the chamber positioned with the chamber and injector reference marks coincident.

Data from all high-response transducers were recorded on an analog tape recorder (CEC VR2600). The tape was subsequently played back for data analysis, generally into an oscillograph using paper speeds as high as 160 in./s. Tape playback speed-reduction factors as high as 64, combined with the high-speed oscillograph, permitted time resolutions as high as 100 μs/in. of record. Shock-tube response tests of these recording and playback methods show an overall rise time capability of about

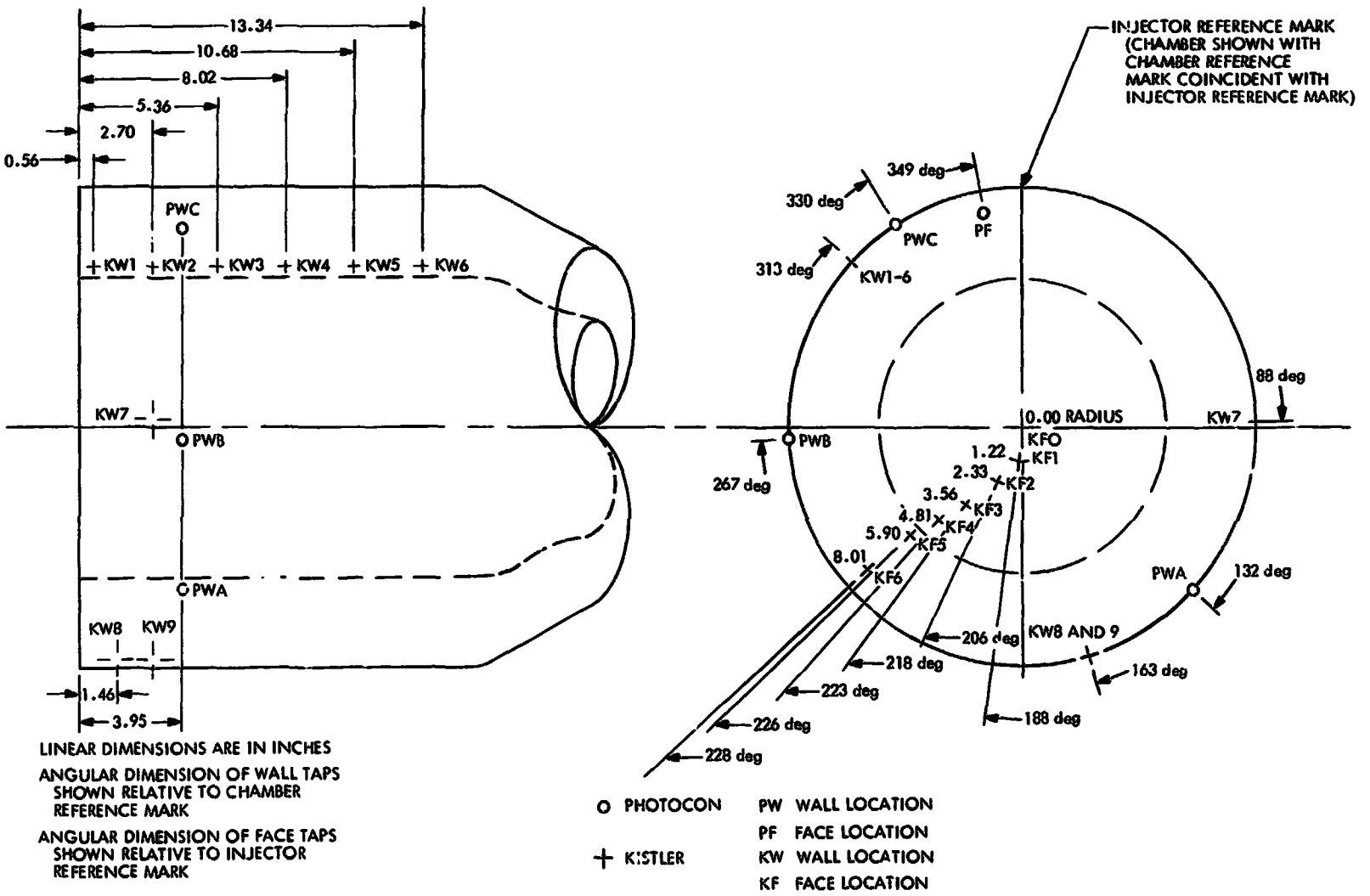

Fig. 8. High-response pressure tap locations, 18-in.-diam cylindrical and annular engines

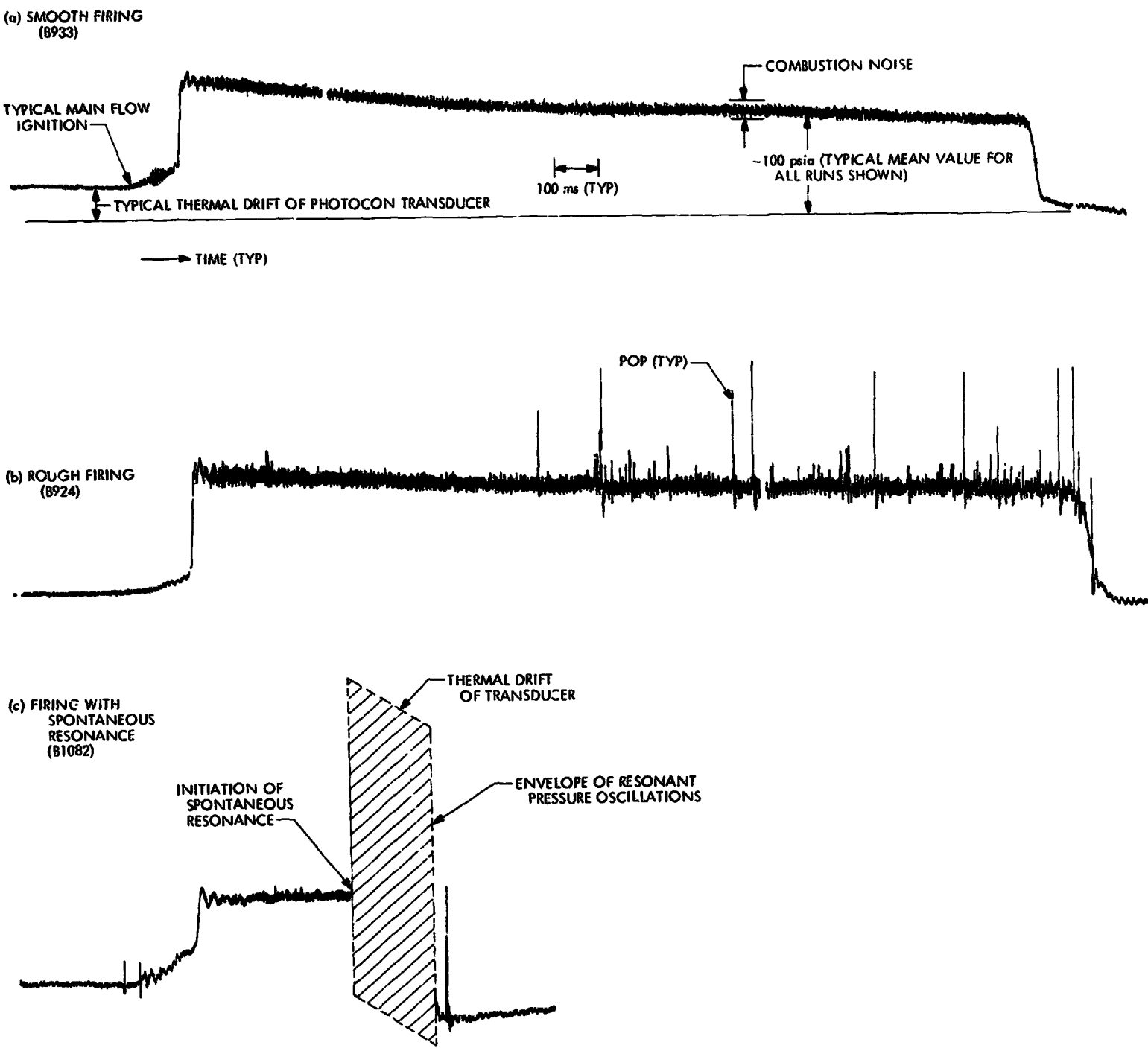

Fig. 9. Typical chamber pressure profiles

6 μs with the Kistler transducer system and a usable frequency response exceeding 80 kHz (see Ref. 18). With the Photocon system, a maximum rise time of ~20 μs and a frequency response of 8 to 10 kHz are realized.

Thus, the transient properties of waves present in the combustion chamber could be studied in considerable detail. Much less detail is required, however, merely to detect the *occurrence of popping;* therefore, relatively few of the highly expanded (and very lengthy) records were made. Instead, much of the high-response data were displayed with a more moderate time expansion of about 50 ms/in. of record. This permitted positive identification of the presence of pops during an entire firing.

D. Description of Typical Firing

The typical runs for which popping data were obtained were short firings of 0.5- to 2-s duration, as dictated by the uncooled engine hardware, instrumentation limitations, or the major objective of the test. Examples of firing profiles of smooth and rough runs are shown in Fig. 9a and 9b, respectively, which illustrate Photocon records of chamber pressure vs time. The mean chamber pressure (and hence, flow rates) achieves what is essentially a steady state within 200 ms of main-flow ignition without significant overshoot, which is the result of the flow control exercised by the relatively slow-opening main propellant valve. Figure 9c shows an analogous profile for a spontaneously resonant firing (no baffles), in which the transition to resonance takes place about 400 ms after main-flow ignition.

III. Results

A. Nature of Pop Disturbance

Portions of Photocon pressure records obtained during the rough combustion exhibited by the *baffled* cylindrical engine are shown in Fig. 10 (using the PF, PWA, and PWB measurements of Fig. 8). The chamber orientation for this run places the wall measurements an additional 80 deg cw from the face measurement compared to that shown in Fig. 8; therefore, the PF and PWB taps are nearly in line, although separated by 3.95 in. axially. Figure 10a illustrates the aperiodic nature of the pops, which frequently exceeded 100 psi above the mean chamber pressure for the baffled chamber. Figure 10b shows the damped behavior of the pressure oscillations induced by pop C (using a somewhat expanded time resolution); it can be seen that the oscillations were damped to nearly the noise-level amplitude in about 6 ms. Pops B and A are shown in still greater detail in Fig. 10c and 10d, respectively. The steep fronted characteristic, which is typical of the pop disturbance, should be noted. The indicated rise time of 15 μs approximates the maximum rise-time resolution of the Photocon system; hence, the actual rate of change of pressure may exceed that shown by these records.

Of additional interest is the fact that, for these three simultaneously recorded pressure measurements, a consistent direction of motion for the recurring pops could not be deduced, indicating that they originated from various locations. For instance, pop A arrived first at the PWB transducer (see Fig. 10d), whereas pop B, occurring at a later time, arrived first at the PWA position. Furthermore, the amplitude of (presumably) the same pop varied considerably as it was sensed by each transducer. These amplitude variations are apparent for pops A, B, and C, but it is difficult to explain them because the spatial origin of the pops and the interference effects of the baffles are unknown.

1. Spatial origin. In an effort to determine the spatial origin of the pops, nine *unbaffled* cylindrical engine firings, which had been made with various arrays of multiple Kistler transducers, were selected for analysis. These runs had undergone spontaneous transitions to resonance after a short period (generally 20 to 50 ms) of smooth combustion.

The initial portion of the transition for one of the firings is shown in Fig. 11, which illustrates the sudden (but not simultaneous) appearance of a large-amplitude disturbance at the nine Kistler transducers (KW1–KW9) and one Photocon transducer (PWB). The chamber reference was oriented 281 deg cw from the injector reference; for convenience, the resulting position of the wall measurements (see Fig. 8) relative to the injector is shown schematically in Fig. 12. Approximately three "cycles" of a wave traveling back and forth across the chamber diameter are shown following the pop in Fig. 11. After about 16 cycles or ~11 ms (not shown), the transition to sustained resonance was complete when a fully developed spinning wave persisted for the remainder of the firing (as shown for the typical resonant run in Fig. 9c). The characteristics of the spinning wave for this engine are described in Ref. 9 and will not be repeated here, except to state that its waveform at the chamber boundaries is essentially the same as that for the initial disturbance shown in Fig. 11; i.e., shock-like.

(a) LOW TIME RESOLUTION RECORD SHOWING RANDOM POPS

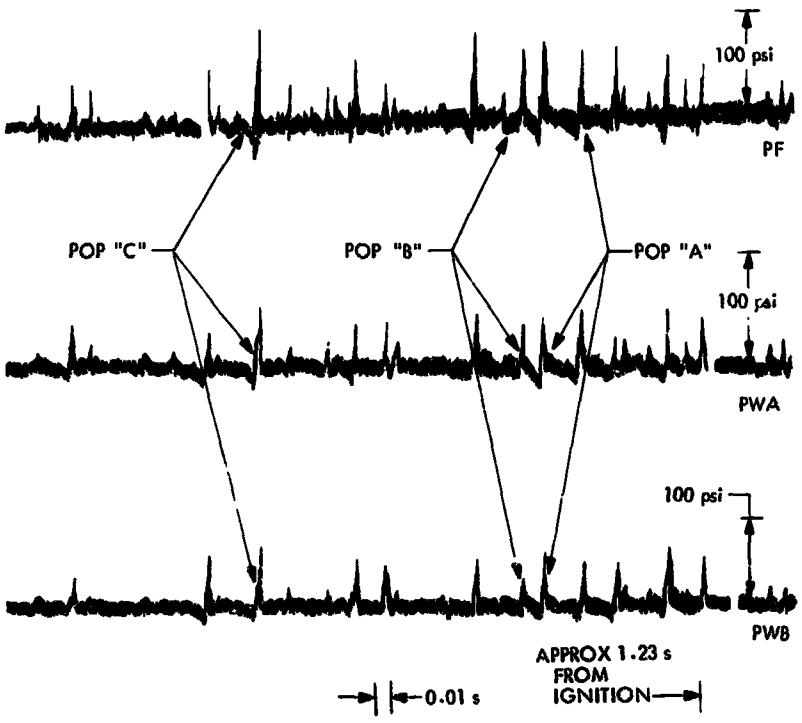

(b) MEDIUM TIME RESOLUTION RECORD SHOWING DAMPING EFFECT OF BAFFLES ON POP "C"

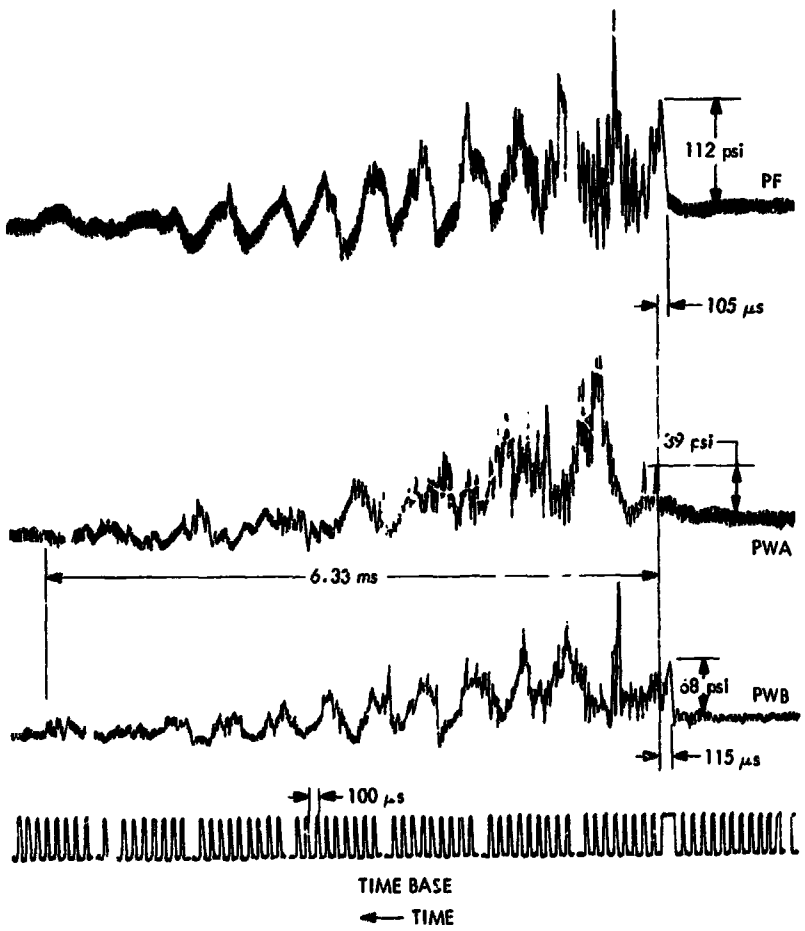

(c) HIGH TIME RESOLUTION RECORD SHOWING FRONTAL CHARACTERISTICS OF POP "B"

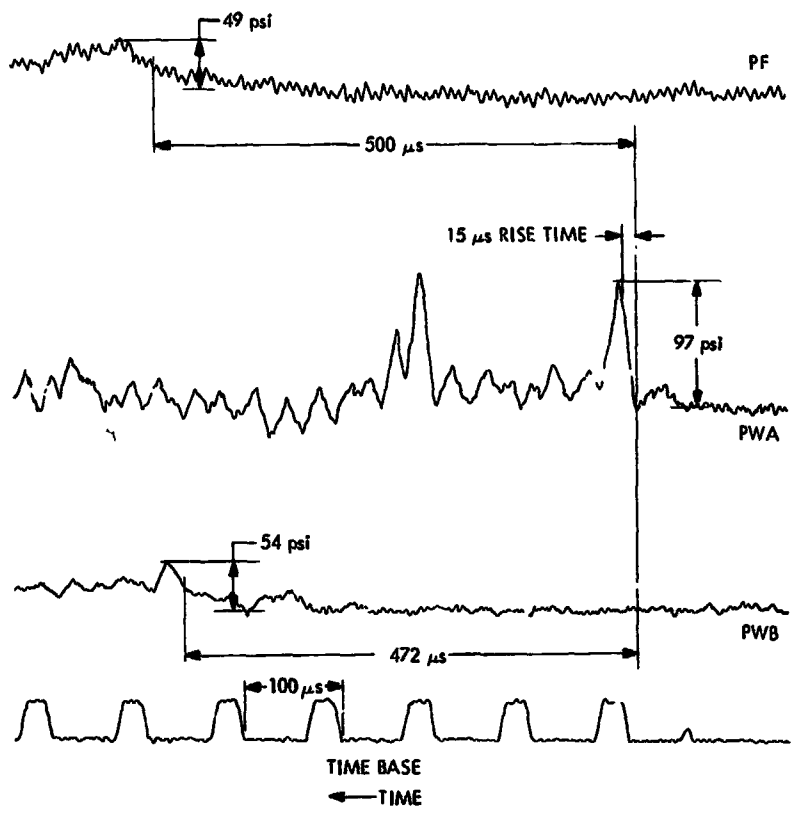

(d) HIGH TIME RESOLUTION RECORD SHOWING FRONTAL CHARACTERISTICS OF POP "A"

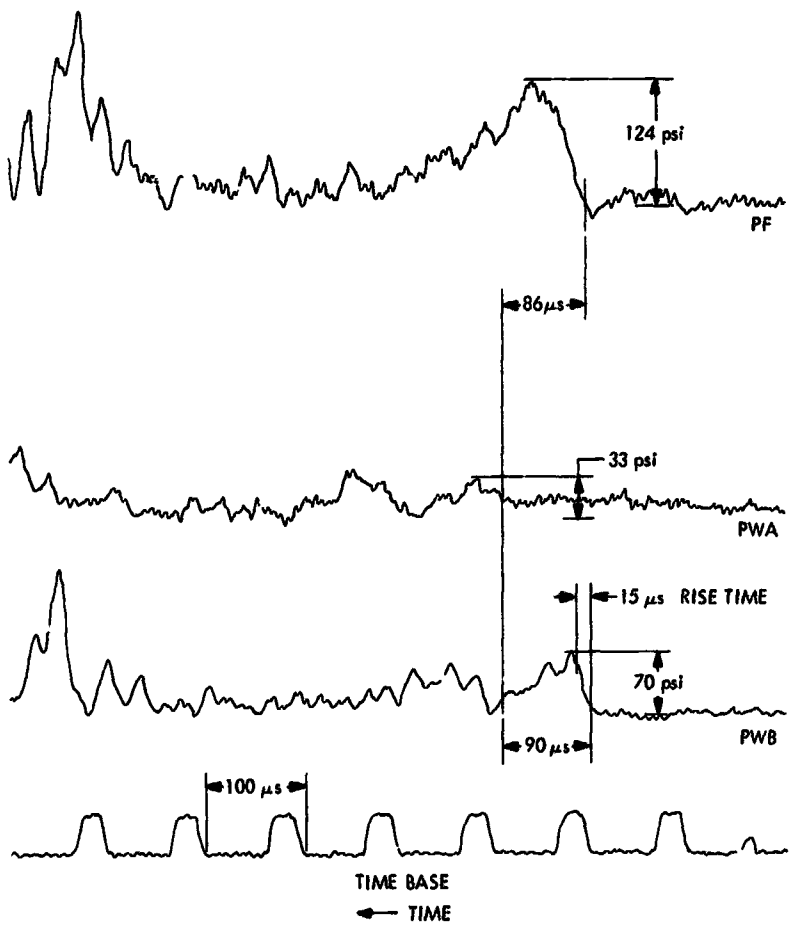

Fig. 10. Pressure vs time records of rough combustion, 18-in.-diam cylindrical engine with baffles, run 922

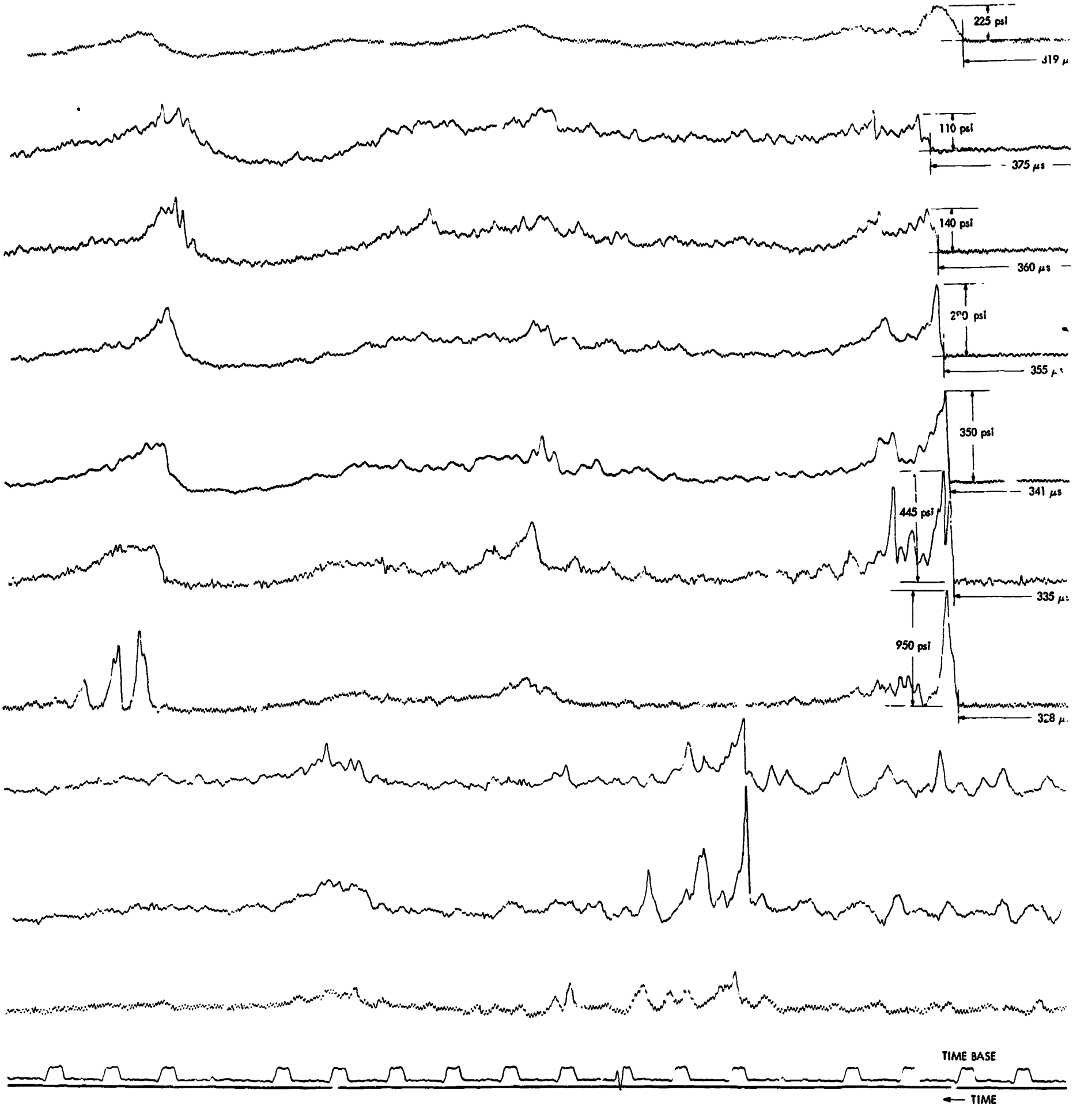

Fig. 11. Pressure distribution along chamber axis vs time for .

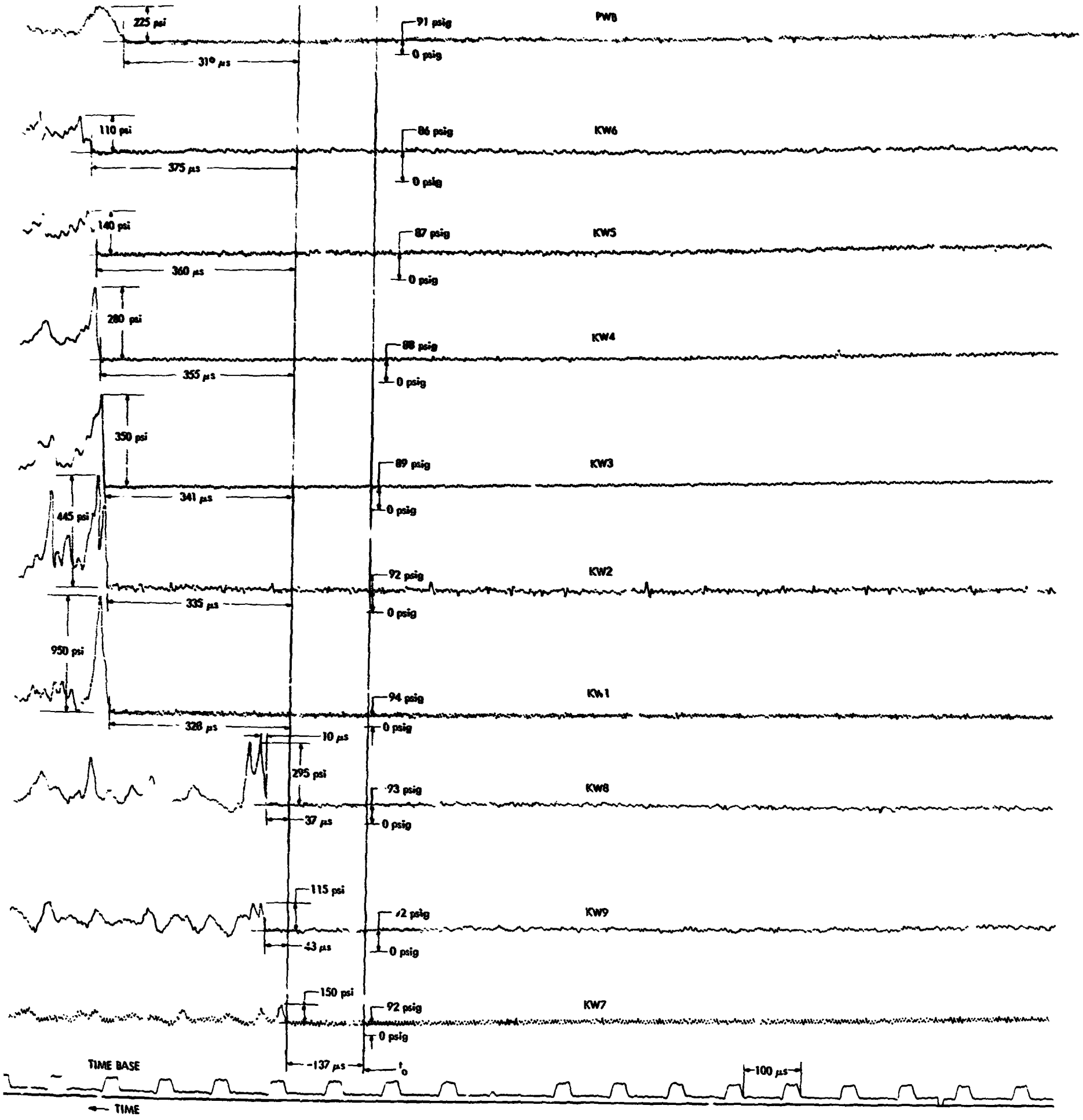

chamber axis vs time for pop-induced resonance, unbaffled 18-in.-diam cylindrical engine with N_2O_4–50/50 (UDMH/N_2H_4) propellants

FOLDOUT FRAME 2

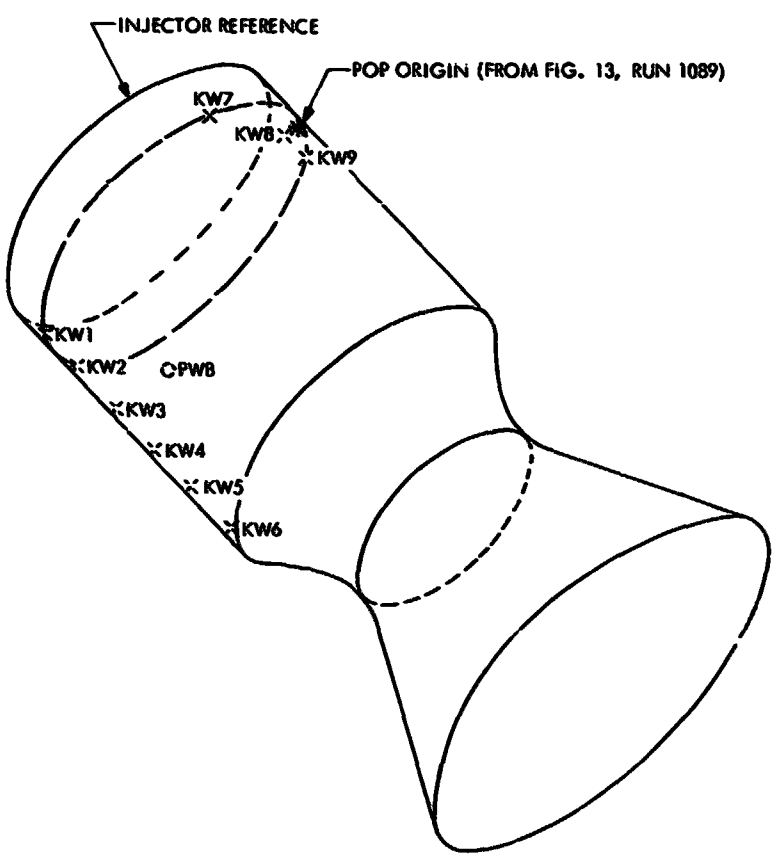

Fig. 12. Position of wall measurements relative to injector (see Fig. 11)

These data serve to illustrate the typical transition to resonance from a pop for this engine, and also the similarity of this type of transition to that of a bomb-induced transition. (See Ref. 5 for a further discussion of the transition to the spinning mode of resonance.)

The method of analysis that was devised for inferring the location of pop origins from measurements such as these was based on the assumption that the pop originates from a particular point in space and time, and that the pressure wave from the disturbance expands spherically at a constant velocity. The following derivation from an analysis by Kushida is taken from Ref. 19:

> The time of origin of the disturbance is denoted by t_0, the position by x_0, y_0, z_0, and the velocity by c. The position of the ith transducer is given by x_i, y_i, z_i and the time of arrival of the pressure wave by t_i, where the subscript i identifies the transducer. We can write an expression equating the distance between the source and a transducer S_i to the distance traveled by the pressure pulse $c(t_i - t_0)$ in the time between initiation and detection. One such equation can be written for each transducer. In the 18-in.-diameter engine, there are generally nine transducers operating simultaneously; hence, there are nine equations. There will be more equations than unknowns (c, t_0, x_0, y_0, z_0), so we shall try to obtain the best fit values for the unknown quantities. We write the equation for the variance ϵ of the position as

$$\epsilon = \frac{1}{N}\sum_{i=1}^{N}[S_i - c(t_i - t_0)]^2 \qquad (1)$$

where the distance S_i is given by

$$S_i = [(x_i - x_0)^2 + (y_i - y_0)^2 + (z_i - z_0)^2]^{1/2} \qquad (2)$$

The values of c, t_0, x_0, y_0, and z_0 which minimize the ϵ are the best fit.

Trial values for the position of the disturbance (x_0, y_0, z_0) are assumed. By differentiating ϵ with respect to c and t_0, while holding position constant, and setting the result equal to zero (i.e., the necessary condition for a minimum), we can derive the following expressions:

$$c = \frac{\overline{St} - \overline{S}\,\overline{t}}{\overline{t^2} - \overline{t}^2} \qquad (3)$$

and

$$t_0 = \overline{t} - \frac{\overline{S}}{c} \qquad (4)$$

where we have defined the mean values

$$\overline{St} \equiv \sum_{i=1}^{N}\frac{S_i t_i}{N}, \qquad \overline{S} \equiv \sum_{i=1}^{N}\frac{S_i}{N}$$

$$\overline{t} \equiv \sum_{i=1}^{N}\frac{t_i}{N}, \qquad \overline{t^2} \equiv \sum_{i=1}^{N}\frac{t_i^2}{N}$$

and N is set equal to the number of data points.

> Note that the times t_0 and t_i are measured from a common, although arbitrary, zero in time. Using Eqs. (2), (3), (4), and then (1), the variance ϵ can be calculated.
>
> The assumed location of the origin is shifted systematically through the volume of the combustion chamber until the position of minimum ϵ is found. This position is taken as the origin of the disturbance.

The credibility of this analysis was verified by applying it to several engine firings during which a small high-explosive bomb (13.5-gr charge) of known location was exploded. The results of this test of the analysis are given in Ref. 19, where it is shown that angular positions within 3 deg and radial positions generally within 1 in. of the actual bomb centerline positions were calculated. These errors are within the volume displaced by the unexploded bomb. Somewhat less accuracy was achieved for the axial position, for which positions from 0.5 to 5.3 in. downstream of the actual location were calculated. It is felt that the latter variability is due to the assumptions of constant wave velocity and sphericity of the expanding wave. Thus, it is concluded that the calculation procedure can give reasonably accurate angular and

radial coordinates of an initial disturbance, but relatively poor axial-position information.

When this procedure was applied to the nine runs selected for pop location analysis, the results shown in Fig. 13 and Table 2 (adapted from Ref. 19) were obtained. The pressure records for run 1103 did not show a definitive initial disturbance, but rather a relatively slow growth of pressure oscillations over many cycles commencing during the starting flow transient; therefore, it was concluded that no pop had occurred, and that the transition to resonance was caused by some other nonsteady combustion condition associated with the start. All of the other eight runs exhibited the pop type of transition after the start transient. Moreover, the calculated pop origins for six of these runs occurred in the region of the chamber boundary. The pops from runs 1089 and 1090 appeared to originate downstream of the same boundary element, but the locations shown for the other runs indicate that the origins were not generally associated with a particular element.

It was thus concluded that, for this engine, pops are initiated through some random process associated with the boundary flow injection scheme, and this conclusion is substantiated by the absence of a pop when no boundary flow was used for run 1103. This absence of pops for the main-flow-only operating condition will be further confirmed later.

Table 2. Calculated coordinates of pop origins relative to injector face

Data point[a]	Run	Calculated coordinates		
		Angle,[b] deg	Radial, in.	Axial, in.
1	1089	40	9.0	4.3
2	1090	38	9.0	9.1
3	1093	115	5.0	14.5
4	1095	157	9.0	9.5
5	1096	150	9.0	11.0
6	1097	169	8.5	7.5
7	1099	22	7.5	11.0
8	1101	327	9.0	3.0
—	1103[c]		Indeterminate	

[a]Indicates data points in Fig. 13.
[b]Clockwise from injector reference mark.
[c]No boundary flow.

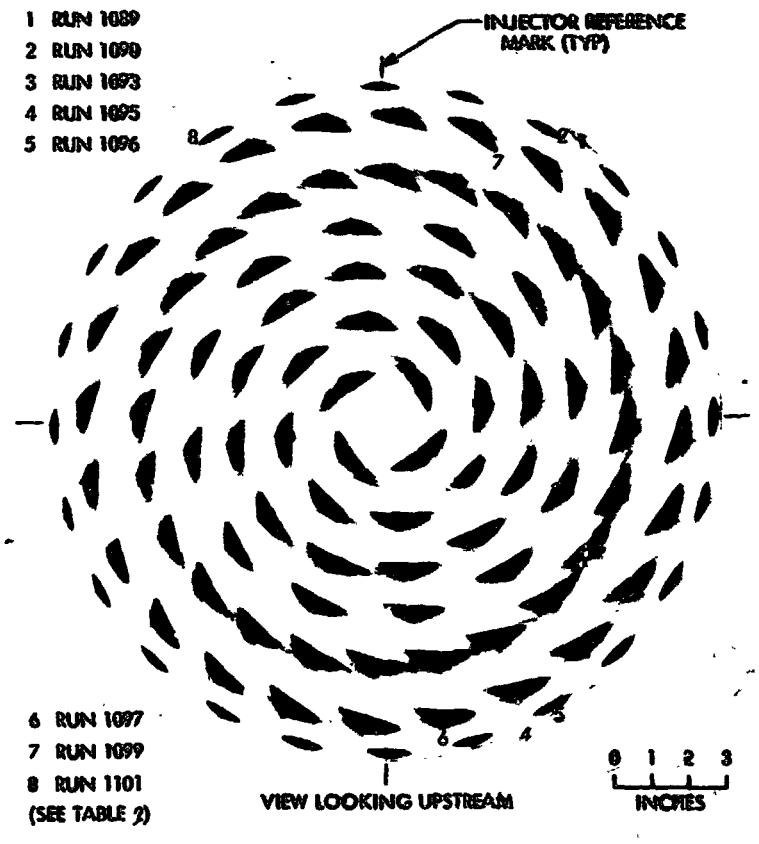

Fig. 13. Locations of pop origins for several runs of unbaffled cylindrical engine

2. Transient behavior. By use of this insight into the spatial position of the pop source and the results of an analysis by Kovitz (see Ref. 6), the pressure records shown in Fig. 11 can now be examined in more detail. Being concerned only with the propagating wave front (assumed to be spherically expanding, as before, and unimpeded by baffles), Kovitz considered that any small segment of the front could be treated as planar. With the further assumption that the advancing front is a Chapman–Jouguet detonation (already developed in the transit time from the origin), the gas properties associated with such a front were calculated for a set of combustion-chamber conditions believed to be realistic within the first half of the chamber length for this engine. These conditions are listed in Table 3. The detonation was taken to be entirely gas-phase (i.e., not two-phase with drops), although the estimated liquid mass was taken into account in the energy released to the front. In this manner, a Mach number of 1.77 and a pressure ratio of 2.17 were calculated for the advancing front. If the velocity of the undisturbed gas ahead of the front is assumed to be zero relative to the direction of front propagation, this Mach number corresponds to a front-propagation velocity of 7140 ft/s across the chamber.

Table 3. Combustion-chamber conditions for detonation calculations

Parameter	Quantity
Overall mixture ratio	2.0
Heat of reaction, cal/g of reactant	1200
Liquid mass fraction[a]	0.50
Ratio of specific heats	1.2
Chamber gas molecular weight	20.4
Chamber gas temperature, °R	5580
Chamber gas pressure, psia	108
Calculated acoustic velocity, ft/s	4030

[a]In first 8 in. of chamber length.

Because it was reasoned that some of the wall-mounted transducers might sense the *reflection* of the front from the wall, the properties of the above wave after a reflection normal to the wall were also calculated by Kovitz. These properties were calculated for two conditions: (1) assuming no temperature gradient near the wall and (2) assuming a relatively cool layer of gas (compared to the combustion gas field) near the wall.

For the case of uniform gas temperature, the predicted reflected overall pressure ratio was 3.67. For the case of a cool gas layer, a significant amplification effect was noted that depended upon the temperature ratio of the hot and cold gases and upon whether or not chemical heat release takes place in the cold gas. With a temperature ratio of 6:1 (realistic for the measured wall temperatures of 200 to 300°F near the injector), the overall reflected pressure ratio was calculated as 3.8 and 6.7, with and without heat release, respectively.

A comparison of these analytical results with some of the experimental measurements shown for run 1089 in Fig. 13 is illustrated in Fig. 14 and Table 4. If it is recalled from the results of the bomb tests that the calculated axial position is generally too far downstream, it can be assumed that the axial position of the pop origin for this run is actually between the 4.3-in. position calculated (from the pop source analysis, Fig. 13 and Table 2) and the injector face. Therefore, the axial position of the pop can be assumed to be near the chamber stations of the KW1, KW2, KW7, KW8, and KW9 transducers. If the cross-sectional volume of the chamber encompassed between the face and the 2.7-in. station of the KW2, KW7, and KW9 transducers is considered to be one-dimensional in the transverse direction, then Fig. 14 illustrates the expanding wave at three positions as it traverses this volume from its origin.

As the front intersects the KW7, KW8, and KW9 transducers, these transducers sense the properties of the advancing front in much the same way as does a side-wall-mounted transducer in a shock tube. However, transducers KW1 and KW2 sense the reflection of the wave as for a shock-tube end-wall measurement. Hence, the pressure ratio sensed at the former locations should be compared to the calculated ratio for the advancing front,

Table 4. Measured and calculated wave properties (run 1089)

Transducer	Pressure ratio		Wave velocity, ft/s	
	Measured	Calculated	Indicated,[a] c	Calculated
KW7	1.55	2.17	3170	7140
KW9	1.22			7140
KW8	2.89			7140
KW2	4.33	3.67 to 6.70[b]	3170	—
KW1	8.93			—

[a]From pop source location analysis.
[b]Depending on assumption of energy release.

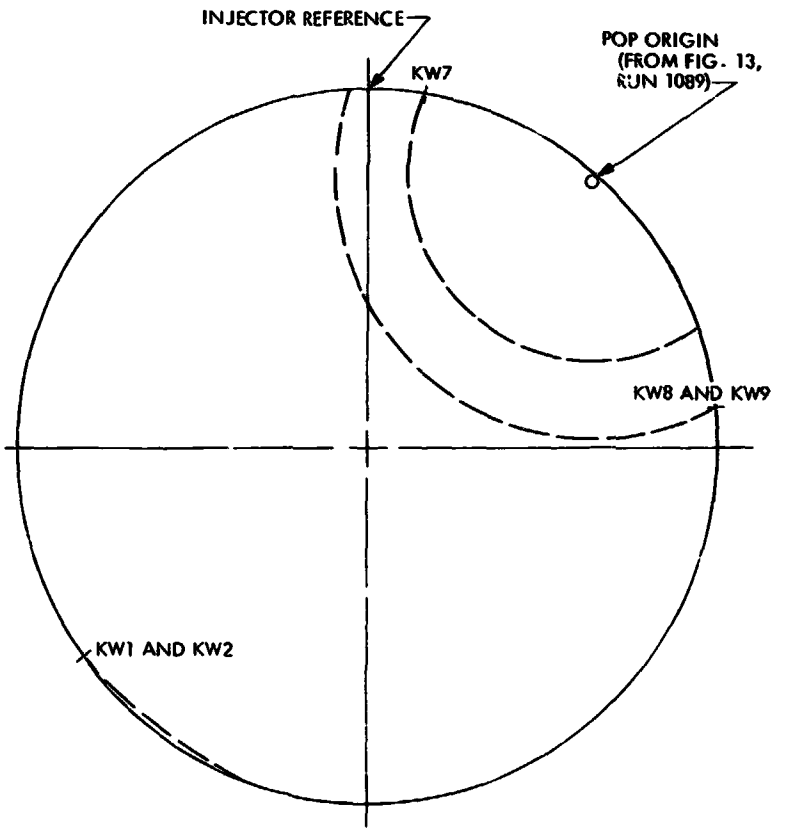

Fig. 14. Schematic of measured and calculated wave properties (run 1089)

whereas that sensed at the latter locations should be compared to the calculated ratios for reflections.

From Table 4, it can be seen that the calculated pressure ratios compare favorably with the respective measured values. However, the transducers located nearer to the face (KW1 and KW8) indicate a higher wave strength than that of the transducers located farther downstream (KW2, KW7, and KW9). This is believed to indicate a complex interaction between the wave and the large combustion gradient (axial direction), which was not considered in the simplified analysis.

A very large difference between calculated and indicated velocity is apparent; however, the indicated velocity is taken from the results of the pop source analysis, which gives only an overall average velocity c for the entire pop disturbance. The source location analysis has already been shown to be weak for locating the axial position of the source, apparently because of the assumptions of disturbance sphericity and constant velocity for all regions of the disturbance. In fact, analogous wave velocities inferred from the bomb tests showed even lower values (~2500 ft/s) than for the spontaneous waves (3170 ft/s).

A crude indication of the magnitude of the difference between the overall average velocity obtained from the pop location analysis and the local velocity near the face can be obtained by comparing the 2500-ft/s average bomb-disturbance velocity with measured bomb-wave velocities (obtained during engine operation). In an ancillary investigation (Ref. 20), the instant of bomb explosion t_o was measured experimentally for a bomb located at the center of the face, and the resulting wave was detected at the chamber wall at the same chamber station as the bomb centerline (the 2.70-in. station for the KW2, KW7, and KW9 transducers). The average transit time of the wave for several measurements was 157.2 μs, which (for the 9.02-in. chamber radius) gives a wave velocity of 4780 ft/s, a factor of 1.91 times the average value inferred from the location analysis. Application of this factor to the average value for the pop disturbance velocity of 3170 ft/s yields a wave velocity of 6060 ft/s near the injector face; this is a more reasonable value, considering the measured pressure ratio of the advancing front, as shown in Table 4.

3. ***Summary of the nature of the pop disturbance.*** Popping is the manifestation of aperiodic, large-amplitude pressure waves propagating through the combustion chamber. In contrast with the normal combustion noise, which is always present, the pop is distinctly singular in that it is one wave that has grown to significantly large strength. This growth, achieved in less time than the transit time of the wave across the chamber, apparently depends upon detonation-like processes rather than on classic acoustic phenomena. The wave usually precipitates sustained, nonlinear, combustion-chamber resonance if the engine is dynamically unstable.

What causes a particular wavelet to grow in this manner and become a pop is not fully understood. However, present experimental evidence shows that the source disturbances originate in the near-wall region of the JPL 18-in.-diam engine—a region associated with the boundary flow injection scheme.

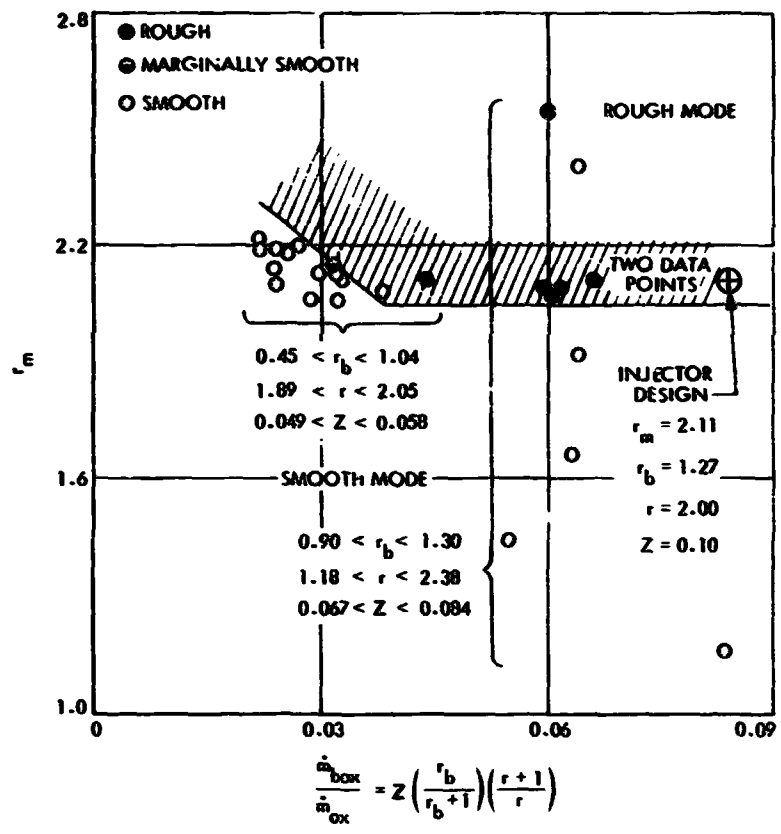

Fig. 15. Early correlation of rough mode with injector operating conditions, 18-in.-diam cylindrical engine with baffles

B. Occurrence of Popping

During early attempts to correlate the occurrence of popping with engine operating conditions, it was noted that the roughness could be eliminated by changing the boundary flow to off-design mixture ratios. Propellant injection temperature was disregarded, but the correlation shown in Fig. 15 (from Ref. 8) was observed for the limited number of firings completed at that time for which popping had been positively identified. A subsequent series of firings (unbaffled cylindrical engine),

with a modified boundary feed and manifolding scheme to enhance the hydraulic stability of the boundary streams, exhibited sporadic occurrences of spontaneously induced resonance, which were attributed to pops. However, the correlation shown in Fig. 15 did not appear to include all of the significant variables of the problem, and the sporadic occurrence of resonance in some cases violated the "smooth" and "rough" regions of that correlation. By the time these firings were completed, it was suspected that propellant temperature was also an important factor; however, since adequate temperature-control facilities were not available at that time, this suspicion could not be clearly verified.

A different series of experiments with the unbaffled annular version of the engine yielded essentially the same spontaneous transitions to resonance as those for the unbaffled cylindrical engine, except that nearly all of the firings were resonant. Stabilizing the annular engine with baffles of adequate length allowed positive identification of the presence of pops. Thus, it seemed clear that the former assumption of a correspondence between the presence of pops and the inception of resonance was verified. It was also noted that these annular-engine firings had been conducted during consistently high ambient air temperature conditions; therefore, propellant temperatures were also consistently high compared to those for the nonresonant cylindrical engine firings. As a consequence, a series of firings was conducted to investigate the temperature effect.

As discussed in Section II-B, propellant temperature-conditioning units were used to isolate the potential effects of the temperature variable. When the results from these experiments were obtained, it became clear that propellant temperature was indeed a primary variable, and efforts were made to assimilate all of the popping data from the cylindrical and annular engine firings into a single correlation. These data, along with the data from the temperature-controlled runs, are listed in Table 5, which divides the many firings into several groups identified primarily on the basis of specific engine configuration and range of flow variations. A summary description of each group is included under "Remarks" in Table 5.

The tabulated boundary mass fraction Z and the mixture ratios r_b and r_m can be compared to the design values listed in Table 1. For convenience of identification, the groups designated with the suffix "A" contain runs with an off-design, main-flow mixture ratio or some other miscellaneous variation (Group XV-A), all other groups are for essentially constant, near-design r_m. Hence, the primary hydraulic variable for the popping data was the boundary flow mixture ratio. Runs of Groups X, XI, and XI-A were conducted with boundary flow deleted.

With the exception of one run in Group XV-A, all of the data are for a chamber pressure of ~100 psia (static pressure), with actual values between 83 and 120 psia. The one exception constituted a cursory examination of the influence of an increased level of combustion pressure on popping. The pressure was elevated to 300 psia by decreasing the nozzle throat area while maintaining the nominal design flow rates.

Most of the runs used nearly equal fuel and oxidizer temperatures (whether temperature-controlled or not), although a substantial temperature difference was present for several runs. The representative combined propellant temperatures (boundary or main) for all firings were taken as a mass-weighted average (assuming equal specific heats) in accordance with the following relationship:

$$\bar{T}_{m,b} = \frac{(T_{m,b})_f + r_{m,b}(T_{m,b})_{ox}}{1 + r_{m,b}}$$

where T is the propellant temperature in the respective manifold during firing; r is the respective mixture ratio ($\dot{m}_{ox}/\dot{m}_f$); and the oxidizer, fuel, main flow, and boundary flow are indicated by subscripts *ox*, *f*, *m*, and *b*, respectively.

If the columns headed by expressions containing p_d/p_{dox} are disregarded for the present, other columns in Table 5 list:

(1) The classification of each run as smooth, marginally smooth, rough, or spontaneously resonant.

(2) A characterization of the rough runs in terms of average popping rate (pops/s).

(3) A measure of the combustion noise for the smooth runs in terms of the rms value of the noise ($p_{c\ rms}$).

The run classification was determined by visual examination of high-response chamber pressure records similar to those shown in Fig. 10a. The following classification definitions were adopted:

(1) Smooth: no pops during firing.

(2) Marginally smooth: one pop during firing.

(3) Rough: more than one pop during firing.

(4) Resonant: spontaneous transition to resonance during firing.

Table 5. Experimental popping data for 18-in.-diam cylindrical and annular engines

Group	Run number	Z	r_b	r_m	p_c (static), psia	T_{mox}, °F	T_{mf}, °F	$\bar{T}_m$, °F	T_{box}, °F	$\bar{T}_{bf}$, °F	T_b, °F	$\left(\frac{p_{df}}{p_{dox}}\right)_m$	$\frac{1}{1+\left(\frac{p_{df}}{p_{dox}}\right)_m}$	$\left(\frac{p_{df}}{p_{dox}}\right)_b$	$\frac{1}{1+\left(\frac{p_{df}}{p_{dox}}\right)_b}$	Run classification[a]	Pops/s	$p_{c\,rms}$, psi rms	η_{c^*}, %	Baffle length (from face), in.
I	924	0.050	1.04	2.08	104	93	102	97.5	93	102	97.5	1.43	0.411	1.47	0.404	R	29.2	—	95.5	2.9
	926	0.057	0.49	2.06	106	98	108	103	98	108	98	1.46	0.406	6.55	0.132	S	0	1.0	96.1	
	927	0.050	0.75	2.13	104	100	103	101.5	100	103	101.5	1.35	0.426	2.78	0.264	S	0	1.1	95.6	
	928	0.048	0.45	2.19	105	104	105	104.5	104	105	104.5	1.28	0.439	7.72	0.115	S	0	1.0	96.6	
	929	0.050	0.78	2.16	104	89	87	88	89	87	88	1.32	0.431	2.62	0.277	S_m	0.5	—	95.7	
	930	0.051	0.55	2.20	104	94	94	94	94	94	94	1.29	0.436	5.20	0.161	S	0	0.9	96.1	
	931	0.049	0.76	2.15	104	96	96	96	96	96	96	1.33	0.429	2.72	0.269	S	0	1.4	95.8	
	932	0.049	0.50	2.20	104	98	97	97.5	98	97	97.5	1.28	0.439	6.30	0.137	S	0	1.1	96.2	
	933	0.047	0.45	2.20	108	103	103	103	103	103	103	1.26	0.443	7.63	0.116	S	0	0.8	95.3	
	934	0.046	0.77	2.13	107	104	104	104	104	104	104	1.35	0.426	2.64	0.275	S	0	0.7	96.0	
	935	0.049	0.49	2.10	107	101	98	99.5	101	98	99.5	1.39	0.418	6.63	0.131	S	0	1.8	96.4	
	936	0.050	0.73	2.06	107	97	100	98.5	97	100	98.5	1.45	0.408	2.96	0.253	S	0	1.5	96.1	
	937	0.050	0.53	2.18	106	92	94	93	92	94	93	1.31	0.433	5.72	0.149	S	0	2.0	95.6	
	938	0.051	0.75	2.11	106	91	91	91	91	91	91	1.39	0.419	2.81	0.263	S	0	1.6	95.8	
	939	0.048	0.49	2.15	105	92	94	93	92	94	93	1.33	0.429	6.55	0.153	S	0	2.2	96.2	
	940	0.058	1.03	2.11	107	92	93	92.5	92	93	92.5	1.39	0.419	1.49	0.401	R	29.0	—	96.6	2.9
	1029	0.055	1.29	1.96	100	61	62	61.5	61	61	61	1.63	0.381	0.96	0.510	Res	—	—	95.5	No baffle
	1031	0.053	1.30	2.09	102	49	47	48	61	59	60	1.45	0.408	0.94	0.514	Res	—	—	94.9	
	1037	0.054	2.10	2.04	100	36	33	34.5	48	46	47	1.50	0.400	0.36	0.734	S	0	0.6	93.5	
	1038	0.054	0.70	2.06	104	51	48	49.5	62	58	60	1.47	0.405	3.24	0.236	S	0	0.8	96.0	
I	1039	0.055	1.42	2.01	100	52	51	51.5	58	59	58.5	1.57	0.389	0.80	0.556	Res	—	—	94.6	No baffle
	Remarks: Cylindrical engine: constant $r_{i,3}$ (near design); constant Z (below design); variable r_b; variable $\bar{T}_b$ (uncontrolled); variable $\bar{T}_m$ (uncontrolled); boundary oxidizer near wall																			
II	1044	0.049	1.36	2.20	104	54	54	54	62	61	61.5	1.29	0.436	0.87	0.534	S	0	0.8	94.0	No baffle
	1047	0.050	1.19	2.15	102	41	40	40.5	48	45	46.5	1.36	0.424	1.13	0.469	S	0	0.9	94.5	
	1049	0.049	0.44	2.13	104	52	51	51.5	62	60	61	1.38	0.420	8.26	0.108	S	0	1.1	95.4	
	1051	0.067	1.07	2.11	96	57	55	56	66	66	66	1.40	0.417	1.60	0.384	Res	—	—	—	
II	1063	0.050	1.95	2.20	104	47	48	47.5	52	50	51	1.30	0.435	0.42	0.703	S	0	0.8	93.8	No baffle
	Remarks: Cylindrical engine: same as Group I except boundary fuel near wall																			
III	913	0.076	1.10	2.07	103	72	72	72	72	72	72	1.45	0.408	1.31	0.433	R	23.6	—	96.4	2.9
III	920	0.079	1.29	2.12	106	78	76	77	78	76	77	1.38	0.420	0.96	0.510	R	40.0	—	96.9	2.9
III	921	0.079	1.28	2.11	108	82	80	81	82	80	81	1.38	0.420	0.96	0.510	R	47.3	—	96.7	2.9

[a]Runs are classified as follows:
S = Smooth (no pops).
S_m = Marginally smooth (one pop during firing).
R = Rough (several to many pops).
Res = Spontaneously resonant.

Table 5 (contd)

Group	Run number	Z	r_b	r_m	p_c (static), psia	T_{mox}, °F	T_{mf}, °F	$\overline{T}_m$, °F	T_{box}, °F	T_{bf}, °F	$\overline{T}_b$, °F	$\left(\frac{p_{df}}{p_{dox}}\right)_m$	$\frac{1}{1+\left(\frac{p_{df}}{p_{dox}}\right)_m}$	$\left(\frac{p_{df}}{p_{dox}}\right)_b$	$\frac{1}{1+\left(\frac{p_{df}}{p_{dox}}\right)_b}$	Run classification[a]	Pop/s	$p_{c\,rms}$, psi rms	η_c, %	Baffle length (from face), in.
III	922	0.073	1.30	2.10	106	72	77	74.5	72	77	74.5	1.42	0.413	0.94	0.514	R	46.8	—	94.4	2.9
III	923	0.077	1.07	2.09	106	91	93	92	91	93	92	1.42	0.413	1.38	0.419	R	17.7	—	97.0	2.9
Remarks: Cylindrical engine: constant r_m (near design); constant Z (below design); variable r_b; variable $\overline{T}_b$ (uncontrolled); variable $\overline{T}_m$ (uncontrolled); boundary oxidizer near wall																				
III-A	914	0.084	1.12	2.41	106	55	51	53	55	51	53	1.08	0.481	1.28	0.440	S	0	0.9	96.9	2.9
↓	915	0.079	1.25	1.92	106	52	46	49	52	46	49	1.69	0.372	1.02	0.495	S	0	1.0	96.0	↓
	916	0.073	1.14	1.67	106	53	55	51.5	53	55	51.5	2.24	0.309	1.23	0.448	S	0	1.0	95.6	
	917	0.067	0.90	1.45	106	50	45	47.5	50	45	47.5	2.98	0.251	1.98	0.335	S	0	0.8	95.7	
↓	918	0.078	1.18	2.55	105	64	59	61.5	64	59	61.5	0.96	0.511	1.15	0.466	R	2.9	—	97.5	↓
III-A	919	0.081	1.24	1.16	102	63	59	61	63	59	61	4.62	0.178	1.04	0.490	S	0	0.8	93.9	2.9
Remarks: Cylindrical engine: same as Group III except variable r_m																				
IV	1032	0.149	1.27	2.15	106	51	49	50	65	63	64	1.35	0.425	1.00	0.500	S	0	0.7	98.3	No baffle
↓	1040	0.152	0.50	2.06	104	57	55	56	60	58	59	1.46	0.407	6.48	0.134	S	0	1.0	95.2	↓
	1041	0.150	1.47	2.06	105	58	58	58	65	65	65	1.48	0.403	0.74	0.573	S	0	0.6	97.5	
IV	1042	0.143	2.17	2.00	100	64	64	64	68	68	68	1.56	0.391	0.34	0.748	Res	—	—	—	No baffle
Remarks: Cylindrical engine: constant r_m (near design); constant Z (above design); variable r_b; variable $\overline{T}_b$ (uncontrolled); variable $\overline{T}_m$ (uncontrolled); boundary oxidizer near wall																				
V	1061	0.145	1.31	2.26	108	47	48	47.5	49	49	49	1.29	0.437	0.94	0.517	S	0	2.0	97.0	No baffle
↓	1064	0.145	2.20	2.23	106	48	48	48	52	51	51.5	1.26	0.443	0.33	0.751	S	0	0.8	95.5	↓
	1065	0.141	0.51	2.26	106	48	48	48	51	52	51.5	1.23	0.449	6.05	0.142	S	0	0.9	94.7	
V	1066	0.145	1.58	2.25	108	48	48	48	51	52	51.5	1.24	0.446	0.64	0.609	S	0	1.2	97.1	No baffle
Remarks: Cylindrical engine: same as Group IV except boundary fuel near wall																				
VI	1002	0.097	1.30	2.09	104	69	69	69	73	71	72	1.43	0.411	0.93	0.520	Res	—	—	—	No baffle
↓	1023	0.104	1.31	2.06	104	69	79	72.5	69	69	69	1.48	0.404	0.93	0.520	S	0	0.4	96.7	↓
	1024	0.096	1.24	2.07	108	48	47	47.5	56	54	55	1.52	0.397	1.04	0.490	S	0	0.6	97.0	
	1026	0.099	1.23	2.12	108	58	58	58	66	66	66	1.39	0.418	1.06	0.486	S	0	0.8	97.5	
	1027	0.099	1.23	2.10	108	61	60	60.5	67	68	67.5	1.42	0.413	1.06	0.486	R	1.5	—	97.6	
	1028	0.107	1.27	2.00	104	62	63	62.5	63	63	63	1.56	0.391	1.00	0.500	R	2.9	—	97.4	
	1033	0.100	1.52	2.07	105	47	44	45.5	51	47	49	1.46	0.407	5.91	0.145	S	0	1.0	95.9	
	1034	0.100	1.53	2.10	105	48	45	46.5	51	51	51	1.42	0.413	0.68	0.594	S_m	0.5	—	96.6	
	1036	0.101	2.14	2.05	102	34	33	33.5	43	42	42.5	1.50	0.400	0.35	0.715	S	0	0.6	95.3	
↓	1082	0.097	1.27	1.99	106	69	68	68.5	70	73	71.5	1.57	0.389	0.98	0.505	Res	—	—	—	↓
VI	1084	0.096	1.23	2.21	106	56	55	55.5	50	65	56	1.28	0.439	1.07	0.483	S	0	0.4	97.2	No baffle

Table 5 (contd)

Group	Run number	Z	r_b	r_m	P_c (static), psia	T_{mox}, °F	T_{mf}, °F	$\overline{T}_m$, °F	T_{box}, °F	T_{bf}, °F	$\overline{T}_b$, °F	$\left(\frac{P_{df}}{P_{dox}}\right)_m$	$\frac{1}{1+\left(\frac{P_{df}}{P_{dox}}\right)_m}$	$\left(\frac{P_{df}}{P_{dox}}\right)_b$	$\frac{1}{1+\left(\frac{P_{df}}{P_{dox}}\right)_b}$	Run classification[a]	Pops/s	$P_{c\,rms}$, psi rms	η_{c^*} %	Baffle length (from face), in.
VI	1087	0.098	1.26	2.09	106	43	56	47.5	44	57	50	1.45	0.408	1.02	0.494	S	0	No rms data	96.9	No baffle
VI	1088	0.099	1.26	2.11	106	42	56	47.5	43	61	51	1.42	0.413	1.02	0.495	S	0	No rms data	97.0	No baffle
Remarks: Cylindrical engine: constant r_m (near design); constant Z (near design); variable r_b; variable $\overline{T}_b$ (uncontrolled); variable $\overline{T}_m$ (uncontrolled); boundary oxidizer near wall																				
VII	1043	0.100	1.44	2.17	106	53	52	52.5	59	58	58.5	1.33	0.429	0.77	0.564	S	0	0.9	95.6	No baffle
↓	1046	0.098	1.23	2.08	104	57	57	57	61	62	61.5	1.44	0.410	1.06	0.485	S	0	1.0	96.3	↓
	1048	0.100	0.46	2.16	104	42	41	41.5	51	51	51	1.35	0.426	7.70	0.115	S	0	1.4	94.4	
	1060	0.096	1.33	2.21	106	48	48	48	48	47	47.5	1.28	0.439	0.91	0.525	S	0	1.1	96.7	
VII	1062	0.097	2.22	2.22	105	46	48	47	51	51	51	1.27	0.440	0.33	0.755	S	0	0.8	94.3	No baffle
Remarks: Cylindrical engine: same as Group VI except boundary fuel near wall																				
VIII	1121	0.156	1.33	2.06	100	61	62	61.5	70	70	70	1.47	0.405	0.90	0.502	Res	—	—	—	No baffle
↓	1122A	0.160	1.35	2.13	102	50	51	50.5	62	61	61.5	1.38	0.420	1.07	0.507	S	0	2.9	—	No baffle
	1203	0.167	1.24	2.14	107	80	79	79.5	94	94	94	1.35	0.426	1.03	0.493	R	47.5	—	94.5	3.9
	1206	0.169	1.32	1.96	100	93	93	93	101	105	103	1.61	0.383	0.91	0.525	Res	—	—	—	3.9
	1207	0.164	1.23	1.97	102	91	89	90	101	102	101.5	1.59	0.386	1.04	0.490	R	35.0	—	—	4.9
	1208	0.163	1.24	2.09	106	95	95	95	98	104	101.5	1.41	0.415	1.03	0.493	R	26.7	—	—	4.9
	1209	0.164	1.24	2.10	106	77	75	76	86	90	88	1.41	0.415	1.04	0.491	R	29.0	—	94.2	4.9
	1211	0.166	1.26	2.05	105	89	88	88.5	95	100	97	1.47	0.405	1.00	0.500	R	23.0	—	95.2	5.4
	1213	0.162	1.26	2.11	105	56	55	55.5	63	62	62.5	1.41	0.415	1.01	0.498	S	0	1.2	94.4	4.4
	1215	0.161	1.22	2.15	104	60	58	59	69	68	68.5	1.35	0.426	1.07	0.505	R	5.9	—	94.1	4.4
VIII	1216	0.150	1.25	1.98	100	85	83	84	91	95	93	1.58	0.388	1.02	0.496	Res	—	—	—	3.9
Remarks: Annular engine: constant r_m (near design); constant Z (near design); constant r_b (near design); variable $\overline{T}_b$ (uncontrolled); variable $\overline{T}_m$ (uncontrolled); boundary oxidizer near wall																				
VIII-A	1198	0.170	1.23	1.63	102	94	95	94.5	102	104	103	2.32	0.301	1.04	0.498	Res	—	—	—	2.9
VIII-A	1199	0.180	1.26	1.65	103	84	83	83.5	91	93	92	2.28	0.305	1.00	0.500	Res	—	—	—	2.9
VIII-A	1202	0.184	1.27	1.69	94	82	81	81.5	92	93	92.5	2.17	0.316	0.98	0.505	Res	—	—	—	2.9
Remarks: Annular engine: constant r_m (below design); constant Z (above design); constant r_b (near design); variable $\overline{T}_b$ (uncontrolled); variable $\overline{T}_m$ (uncontrolled); boundary oxidizer near wall																				
IX	1220	0.163	1.35	2.21	101	46	44	45	44	44	44	1.30	0.435	0.91	0.524	S	0	2.2	93.3	4.9
IX	1221	0.166	1.33	2.20	102	52	52	52	71	102	84	1.29	0.437	0.92	0.521	R	18.7	—	97.9	4.9

Table 5 (contd)

Group	Run number	Z	r_b	r_m	p_c (static), psia	T_{mox}, °F	T_{mf}, °F	$\bar{T}_m$, °F	T_{box}, °F	T_{bf}, °F	$\bar{T}_b$, °F	$\left(\frac{p_{df}}{p_{dox}}\right)_m$	$\frac{1}{1+\left(\frac{p_{df}}{p_{dox}}\right)_m}$	$\left(\frac{p_{df}}{p_{dox}}\right)_b$	$\frac{1}{1+\left(\frac{p_{df}}{p_{dox}}\right)_b}$	Run classification[a]	Pop/s	$p_{c\,rms}$, psi rms	η_c, %	Baffle length (from face), in.
IX	1222	0.171	1.27	2.02	104	51	52	51.5	35	36	35.5	1.54	0.394	1.00	0.500	S	0	1.8	93.7	4.9
	1224	0.167	1.27	2.10	104	51	53	52	57	107	79	1.42	0.413	1.03	0.494	R	15.3	—	94.6	
	1225	0.167	1.33	2.12	103	41	41	41	48	71	58	1.34	0.427	0.92	0.521	S	0	1.2	93.3	
	1226	0.171	1.32	2.11	104	41	42	41.5	49	91	67	1.45	0.408	0.95	0.514	R	3.3	—	96.2	
	1227	0.166	1.28	2.08	103	48	47	47.5	57	64	60	1.45	0.408	0.98	0.506	S	0	1.7	94.0	
	1228	0.167	0.92	2.05	106	55	55	55	57	94	76	1.44	0.410	1.98	0.335	S	0	2.0	94.4	
	1229	0.168	0.75	2.08	106	55	55	55	57	91	76.5	1.44	0.410	2.92	0.256	S_m	0.5	—	94.2	
	1231	0.163	2.82	2.13	100	56	57	56.5	60	107	72.5	1.38	0.420	0.21	0.829	S	0	1.5	89.8	
	1232	0.163	2.39	2.18	101	56	57	56.5	57	95	68.5	1.31	0.433	0.28	0.780	R	4.3	—	90.8	
	1233	0.168	0.77	2.08	106	60	62	61	84	103	95	1.44	0.410	2.71	0.269	S	0	1.0	94.3	
	1234	0.167	1.59	2.04	103	60	61	60.5	88.5	116.5	99	1.50	0.400	0.64	0.611	R	6.1	—	92.5	
	1235	0.166	1.80	2.11	101	46	47	46.5	92	106	97	1.41	0.415	0.49	0.671	R	1.0	—	91.9	
	1236	0.164	1.01	2.10	104	49	49	49	86	106	96	1.43	0.412	1.56	0.391	R	8.9	—	97.2	
	1237	0.163	1.98	2.10	101	49	48	48.5	87	95	90	1.41	0.415	0.41	0.712	S	0	1.0	91.2	
	1238	0.164	1.57	2.11	103	55	55	55	81	92	85	1.41	0.415	0.65	0.608	R	4.3	—	92.6	
	1239	0.166	1.58	2.08	103	53	55	54	68	85	74.5	1.45	0.408	0.65	0.606	R	2.5	—	93.2	
	1240	0.163	1.84	2.10	102	49	49	49	80	86	82	1.43	0.412	0.47	0.682	S	0	0.9	92.6	
	1241	0.163	1.83	2.09	102	50	50	50	72	81	75.5	1.44	0.410	0.48	0.676	S_m	0.5	—	92.5	
	1242	0.164	0.92	2.06	105	52	53	52.5	64.5	74	69.5	1.48	0.403	1.91	0.344	S	0	0.9	94.5	
	1243	0.165	0.92	2.04	104	50	50	50	61	66	63.5	1.50	0.400	1.89	0.346	S	0	0.8	94.5	
	1244	0.165	1.82	2.05	101	49	51	50	63	66.5	65	1.49	0.401	0.48	0.674	S	0	0.8	92.0	
	1245	0.165	1.33	2.02	104	47	46	46.5	84	46	67.5	1.55	0.392	0.89	0.531	S	0	0.8	93.5	
	1246	0.165	1.34	2.06	103	47	49	48	69.5	47	60	1.48	0.403	0.88	0.532	S_m	0.5	—	93.3	
	1249	0.165	1.30	2.07	105	53	51.5	52.5	91.5	50	73.5	1.44	0.410	0.92	0.521	S	0	0.8	93.8	
	1253	0.163	1.25	2.10	104	63	58	60.5	97	74	87	1.42	0.414	1.00	0.501	R	3.0	—	93.8	
IX	1256	0.166	1.22	2.10	106	68	67	67.5	96.5	116	105	1.40	0.417	1.08	0.480	R	2[illegible].0	—	94.5	4.9
Remarks: Annular engine: constant r_m (near design); constant Z (near design); variable r_b; variable $\bar{T}_b$ (controlled); variable $\bar{T}_m$ (uncontrolled); boundary oxidizer near wall																				
IX-A	1258	0.160	0.44	2.50	106	100	114	103	69	71	70	1.00	0.500	8.27	0.108	S	0	1.1	94.9	4.9
	1259	0.163	0.49	3.04	104	95	107	98	74	71	72.5	0.67	0.599	6.59	0.132	R	2.3	—	92.6	
	1261	0.166	0.49	2.45	105	68	63	65.5	69	68	68.5	1.04	0.492	6.73	0.129	S	0	1.2	92.7	
	1262	0.168	0.49	2.94	103	72	72	72	69	68	68.5	0.72	0.581	6.59	0.132	R	4.7	—	96.6	
	1265	0.167	0.52	3.06	101	50	49.5	50	66	65	65.5	0.67	0.599	5.99	0.143	S	0	0.8	91.1	
	1266	0.163	1.27	2.98	103	101	106	103.5	106	88	98.5	0.70	0.590	0.96	0.509	R	8.3	—	95.2	
IX-A	1267	.159	1.26	1.56	110	92	109	98.5	99	85	93	2.56	0.281	0.98	0.504	R	17.7	—	96.2	4.9
Remarks: Annular engine: variable r_m; constant Z (near design); variable r_b; variable $\bar{T}_b$ and $\bar{T}_m$—either or both controlled; boundary oxidizer near wall																				
X	943	—	—	2.14	95	101	101	101	—	—	—	1.36	0.423	—	—	S	0	1.3	93.1	2.9
X	944	—	—	2.13	96	101	100	100.5	—	—	—	1.38	0.421	—	—	S	0	1.2	92.9	2.9
X	1030	—	—	2.00	83	53	51	52	—	—	—	1.57	0.390	—	—	S	0	0.3	91.1	No baffle

Table 5 (contd)

Group	Run number	Z	r_b	r_m	P_c (static), psia	T_{mox}, °F	T_{mf}, °F	$\overline{T}_m$, °F	T_{box}, °F	T_{bf}, °F	$\overline{T}_b$, °F	$\left(\frac{P_{df}}{P_{dox}}\right)_m$	$\frac{1}{1+\left(\frac{P_{df}}{P_{dox}}\right)_m}$	$\left(\frac{P_{df}}{P_{dox}}\right)_b$	$\frac{1}{1+\left(\frac{P_{df}}{P_{dox}}\right)_b}$	Run classification[a]	Pops/s	$P_{c\text{-}rms}$, psi rms	η_{c^*}, %	Baffle length (from face), in.
X	1035	—	—	2.08	100	53	52	52.5	—	—	—	1.45	0.409	—	—	S	0	0.7	92.8	No baffle
↓	1059	—	—	2.16	102	45	47	46	—	—	—	1.35	0.426	—	—	S	0	0.8	93.0	↓
↓	1072	—	—	2.07	96	47	45	46	—	—	—	1.47	0.406	—	—	S	0	0.6	92.1	↓
X	1102	—	—	2.04	94	92	94	93	—	—	—	1.44	0.411	—	—	S	0	No rms data	—	No baffle
Remarks: Cylindrical engine; constant r_m (near design); main flow only; variable $\overline{T}_m$ (uncontrolled)																				
XI	1210	—	—	2.04	85	87	87	87	—	—	—	1.49	0.402	—	—	S	0	3.0	87.4	4.9
XI	1212	—	—	2.07	85	85	89	87	—	—	—	1.45	0.408	—	—	S	0	2.8	87.5	5.4
XI	1217	—	—	2.06	91	86	85	85.5	—	—	—	1.46	0.406	—	—	S	0	4.2	88.9	3.9
Remarks: Annular engine: constant r_m (near design); main flow only; constant $\overline{T}_m$ (uncontrolled)																				
XI-A	1247	—	—	2.48	102	52	49	50.5	—	—	—	1.01	0.497	—	—	S	0	0.8	87.3	4.9
↓	1248	—	—	2.92	101	51	49.5	50.5	—	—	—	0.74	0.577	—	—	S	0	0.9	88.9	↓
↓	1257	—	—	2.50	104	101	94	99	—	—	—	0.99	0.489	—	—	S	0	1.5	87.9	↓
↓	1260	—	—	3.01	103	95	101	96.5	—	—	—	0.68	0.593	—	—	S	0	1.4	89.7	↓
↓	1263	—	—	2.52	103	77	73	75	—	—	—	0.98	0.504	—	—	S	0	1.3	87.3	↓
XI-A	1264	—	—	2.98	101	75	73	74	—	—	—	0.70	0.589	—	—	S	0	1.0	89.2	4.9
Remarks: Annular engine: variable r_m; main flow only; variable $\overline{T}_m$ (controlled)																				
XII	1067	0.022	—	2.04	102	62	59	60.5	—	63	63	1.50	0.400	~1.0[b]	~0.50	S	0	0.9	94.9	No baffle
XII	1074	0.029	—	2.05	~100	52	51	51.5	—	60	60	~1.5	~0.40	~1.0[b]	~0.50	S	0	0.8	95.5	No baffle
XII	1075	0.046	—	2.06	~100	52	50	51	—	61	61	~1.5	~0.40	~1.0[b]	~0.50	S	0	1.1	97.2	No baffle
Remarks: Cylindrical engine: constant r_m (near design); variable Z; variable $\overline{T}_b$ (uncontrolled); variable $\overline{T}_m$ (uncontrolled); boundary fuel only																				
XIII	1254	0.087	—	2.08	99	68	67	67.5	—	86	86	1.44	0.410	~1.0[b]	~0.50	R	9.5	—	96.4	4.9
XIII	1268	0.078	—	2.08	98	74.5	75	75	—	108.5	108.5	1.43	0.412	~2.75[b]	0.267	S	0	1.7	95.0	4.9
Remarks: Annular engine: constant r_m (near design); constant Z; variable $\overline{T}_b$ (controlled); variable $\overline{T}_m$ (uncontrolled); boundary fuel only																				
XIV	1077	0.047	—	2.01	96	73	73	73	77	—	77	1.54	0.394	~1.0[b]	~0.50	S	0	1.4	90.1	No baffle
XIV	1079	0.040	—	2.00	97	74	75	74.5	70	—	70	1.56	0.391	~1.0[b]	~0.50	S	0	1.4	90.9	No baffle

[b] P_{df}/P_{dox} is defined as ratio of inner to outer stream dynamic pressures for runs with single-propellant boundary flow.

Table 5 (contd)

Group	Run number	Z	r_b	r_m	p_c (static), psia	T_{mox}, °F	T_{mf}, °F	$\bar{T}_m$, °F	T_{box}, °F	T_{bf}, °F	$\bar{T}_b$, °F	$\left(\frac{p_{df}}{p_{dox}}\right)_m$	$\frac{1}{1+\left(\frac{p_{df}}{p_{dox}}\right)_m}$	$\left(\frac{p_{df}}{p_{dox}}\right)_b$	$\frac{1}{1+\left(\frac{p_{df}}{p_{dox}}\right)_b}$	Run classification[a]	Pop/s	$p_{c\,rms}$, psi rms	η_{c^*}, %	Baffle length (from face), in.
XIV	1080	0.069	—	2.02	95	73	76	74.5	70	—	70	1.53	0.395	~1.0[b]	~0.50	S	0	1.5	89.7	No baffle
	Remarks: Cylindrical engine: same as Group XII, except boundary oxidizer only																			
XV-A	1250	1.0	1.45	—	17	—	—	—	72	102.5	84.5	—	—	0.78	0.563	S	0	Nil	—	4.9
↓	1251	0.160	1.18[c]	2.08	102	63	63	63	85	89	87	1.45	0.408	0.91	0.523	R & Res	6.1 (weak)	—	—	↓
	1252	0.164	1.13[c]	2.04	101	64	64	64	72	74	73	1.49	0.402	0.99	0.502	Res	—	—	—	
	1255	0.164	1.26	2.17	302	73	72	72.5	83	98	89.5	1.32	0.432	0.96	0.511	S	0	0.9	—	
	1269[d]	0.0065	1.29	—	105	—	—	—	85	82.5	84	—	—	0.95	0.512	R	8	—	—	
XV-A	1269[e]	0.167	0.44	2.14	105	73	71	72	81	81	81	1.36	0.424	8.28	0.108	—	—	—	—	4.9
	Remarks *Annular engine: miscellaneous experiments; boundary flow only (run 1250); propellant substitution (runs 1251 and 1252); high chamber pressure (run 1255); single boundary element separately controlled (run 1269)*																			

[c]Furfuryl alcohol substituted for boundary fuel.

[d]Data for single (separately controlled) boundary element.

[e]Data for remaining 23 boundary elements and main elements.

For present purposes, roughness associated with the start transient and transitions to resonance occurring during the start were not considered in the popping data.

Because identification of individual pops is a matter of judgment when many pops are present (see Fig. 10), the average popping rate is admittedly a coarse measure of popping. However, any bona fide pop could be discerned on all pressure records for a given run, and, because the run classifications and popping rates for these data were assigned by one individual, there is relative significance within the data.

The rms value of chamber-pressure fluctuations as a useful measure of popping was discarded because the electronic averaging device used a fixed time constant that is short relative to the popping rate. Hence, $p_{c\,\mathrm{rms}}$ does not provide a single representative value that is easily comparable from one popping run to the next, wherein the popping rate may differ by an order of magnitude. It is a useful indicator of normal combustion noise level, however, where the noise frequency is distributed fairly uniformly across the measurable spectrum; therefore, $p_{c\,\mathrm{rms}}$ is included in Table 5 as a characteristic of the smooth runs

Combustion efficiency η_c for most of the nonresonant runs is also listed in Table 5. This parameter is defined as $100(c^*/c^*_{th})$, where c^* is the characteristic velocity (computed from the measured flowrates, and nozzle-entrance static chamber pressure converted to throat stagnation conditions), and c^*_{th} is the theoretical equilibrium characteristic velocity based on overall mixture ratio.

Popping rate vs r_b for several ranges of $\bar{T}_b$ for those runs in Groups I–IX (i.e., those runs maintaining an essentially constant r_m near the design value—see Table 5) where nearly equal fuel and oxidizer temperatures ($\Delta T \leq 10°F$) were present at the boundary, is shown in Fig. 16. The occurrence of popping, as well as the maximum popping rate, tends to be centered around the design (mixing-uniformity) mixture ratio of 1.27 whenever $\bar{T}_b$ is greater than about 60°F.

For mixture ratios near 1.27 in the $\bar{T}_b$ range of 61 to 70°F, popping occurred somewhat sporadically from run to run. When it did occur, the rate was lower by an order of magnitude than the rate for those firings with higher temperatures. Temperatures in the range of 71 to 90°F produced the maximum pop rates (of the order of 45 pops/s), whereas the highest $\bar{T}_b$ range of 91 to 105°F showed

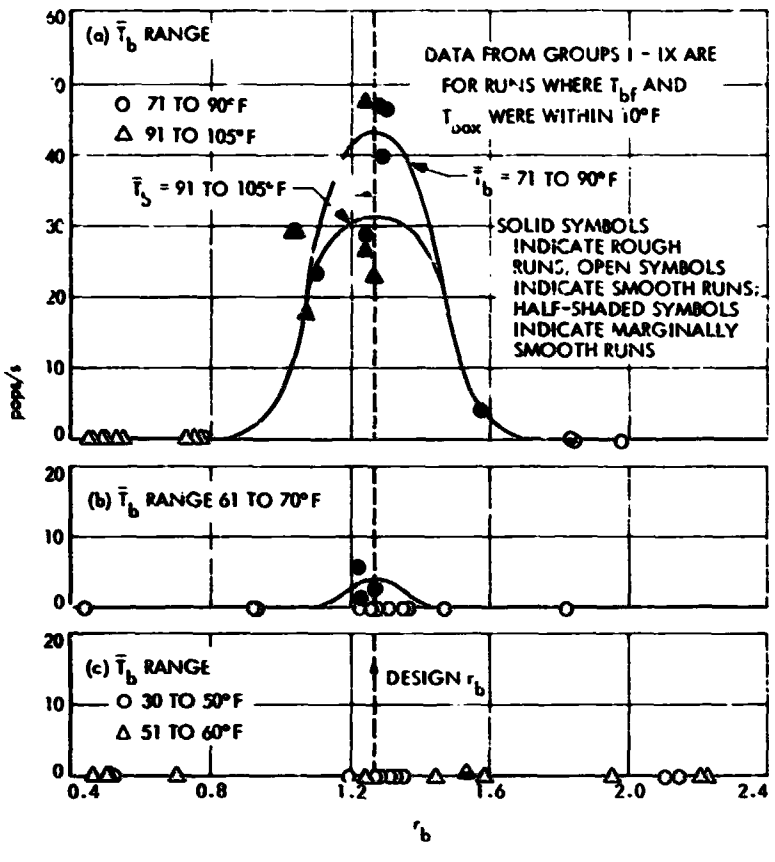

Fig. 16. Popping rate vs r_b for several ranges of $\bar{T}_b$

a tendency to yield somewhat lower rates. The abrupt rise in popping rate to a maximum at about 75°F and the trend toward decreased rates for $\bar{T}_b > 80°F$ are indicated in Fig. 17a, which shows data for a narrow r_b range ($1.19 < r_b < 1.36$) around the design value of 1.27. It should be noted that the higher $\bar{T}_b$ firings are for the annular engine only; therefore, there could be some question as to whether the indicated trend of decreased popping rate for $\bar{T}_b > 80°F$ is fortuitous. However, there is no indication of a different popping-rate behavior between the two engines from other data in Table 5, so this trend is believed to be valid.

Figure 17b shows $p_{c\,\mathrm{rms}}$ vs $\bar{T}_b$ for the smooth firings of runs of these same groups. There is a measurable difference here between the cylindrical and annular engines, with the latter yielding somewhat higher levels of combustion noise, as was mentioned in Section II-A. However, no significant variation in $p_{c\,\mathrm{rms}}$ with $\bar{T}_b$ is observed for either engine. Also, no significant variation in combustion efficiency was observed with increasing $\bar{T}_b$ for these smooth runs, as depicted in Fig. 18. When η_c is taken as a continuous function of $\bar{T}_b$ into the popping regime, a slight increase ($\sim 1\%$) is indicated from the lowest to the highest temperatures encountered—at least for the annular chamber (analogous data are not available for the cylindrical engine).

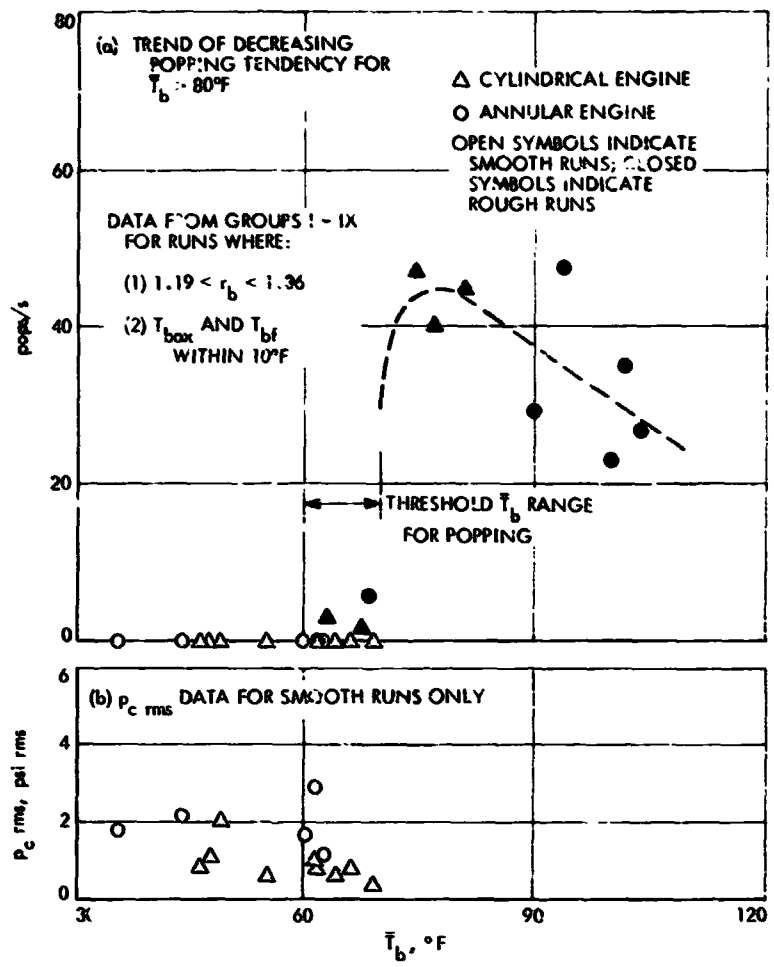

Fig. 17. Popping rate and $p_{c\ rms}$ vs $\bar{T}_b$ for r_b near 1.27

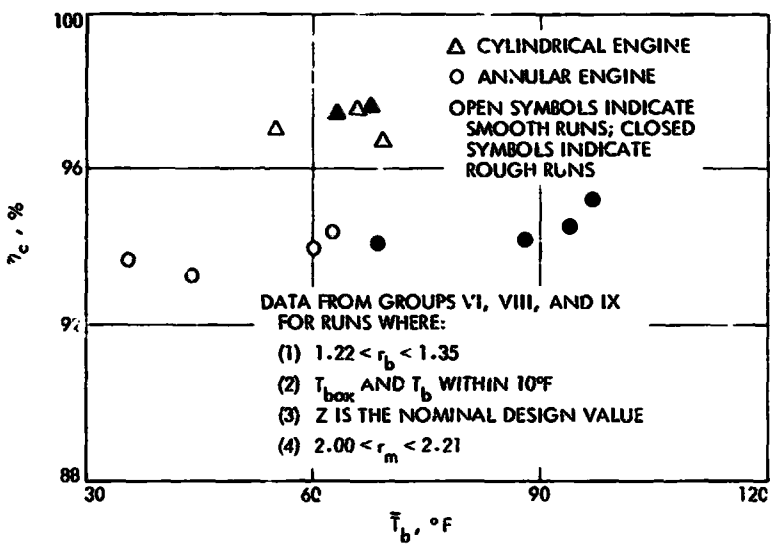

Fig. 18. Combustion efficiency vs $\bar{T}_b$ for r_b near 1.27

By the use of some imagination in combining the information from Figs. 16 and 17a, an "operating map" can be plotted for these engines, such as that shown in Fig. 19. This is a three-dimensional presentation of popping occurrence vs r_b and $\bar{T}_b$, where contours of essentially constant popping rates have been estimated from the popping-rate data. To show how all of the data from Group I–IX (restricted only by the $\Delta T \leq 10°F$ limitation) fit the plot, data for each group are individually identified. The outermost contour line indicates, semiquantitatively, the threshold conditions for popping for this particular injection scheme (the composite main/bipropellant boundary systems) and propellant combination at 100-psia combustion pressure.

As noted earlier in this subsection, some firings were conducted with unequal boundary fuel and oxidizer temperatures. These data, combined with the data used for Fig. 17a ($1.19 < r_b < 1.36$ for all data), are shown in Fig. 20, which shows popping occurrence vs T_{bf} and T_{box}. Lines representing constant values of $\bar{T}_b$ for $r_b = 1.27$ lie diagonally across the plot for reference. Inclusion of the popping rates for the rough runs provides a third dimension to this plot, as was done for Fig. 19. The unsymmetrical orientation of the contour lines connecting approximately equal popping rates, and the estimated outer contour, indicates that popping may be somewhat more sensitive to fuel temperature than to oxidizer temperature.

The data presented thus far have dealt with operation of the two engines with the main flow at the nominal design condition, but with variations in bipropellant boundary flow. Firings with simultaneous variations in r_m and r_b—categorized as Groups III-A, VIII-A, and IX-A—are shown in Fig. 21. The runs are classified as smooth, rough, or resonant, as before. Except for the two runs identified by run numbers 1259 and 1262, each result is consistent with the popping-threshold curves of Figs. 19 and 20, based on r_b and $\bar{T}_b$ only. The two exceptions cannot be explained on the basis of boundary flow alone; however, run 1259 exhibited substantially lower-amplitude pop disturbances than normal, at a relatively low rate, and it is questionable even to identify them as pops. On the other hand, run 1262 produced the normal pop amplitude (still at a relatively low rate) for which no explanation is apparent.

A similar display for *all* firings of Groups I–IX (including the "A" groups) is shown in Fig. 22, with exceptions again noted by run numbers. Run data for the exceptions are listed in Table 6. Of 112 runs, only 5 failed to meet the popping limits prescribed in Figs. 19 and 20. Thus, nearly 96% of the data studied fits the popping-threshold curves deduced from the boundary flow conditions alone.

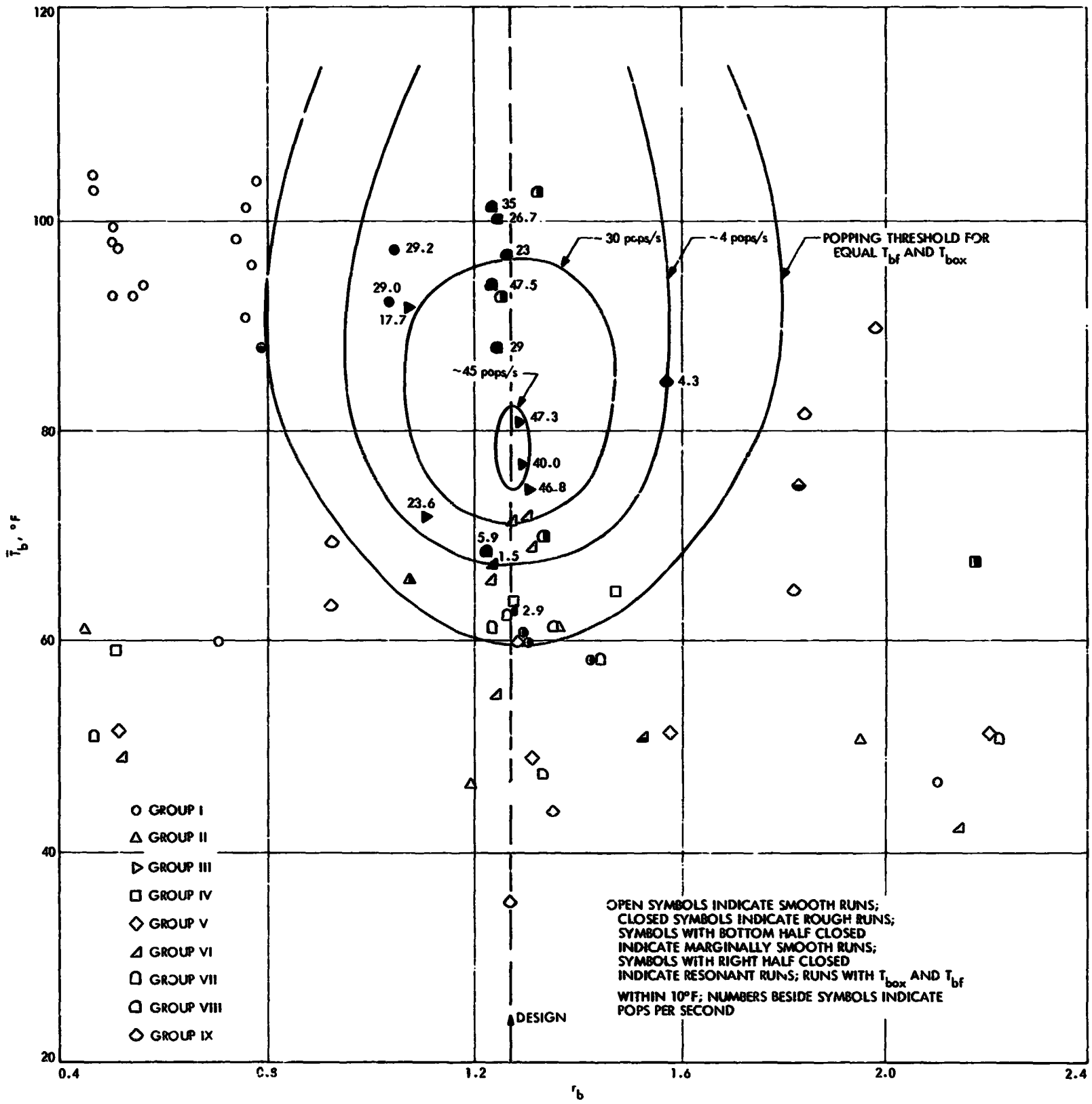

Fig 19. Popping occurrence vs $\bar{T}_b$ and r_b, showing dependence of popping on boundary flow conditions

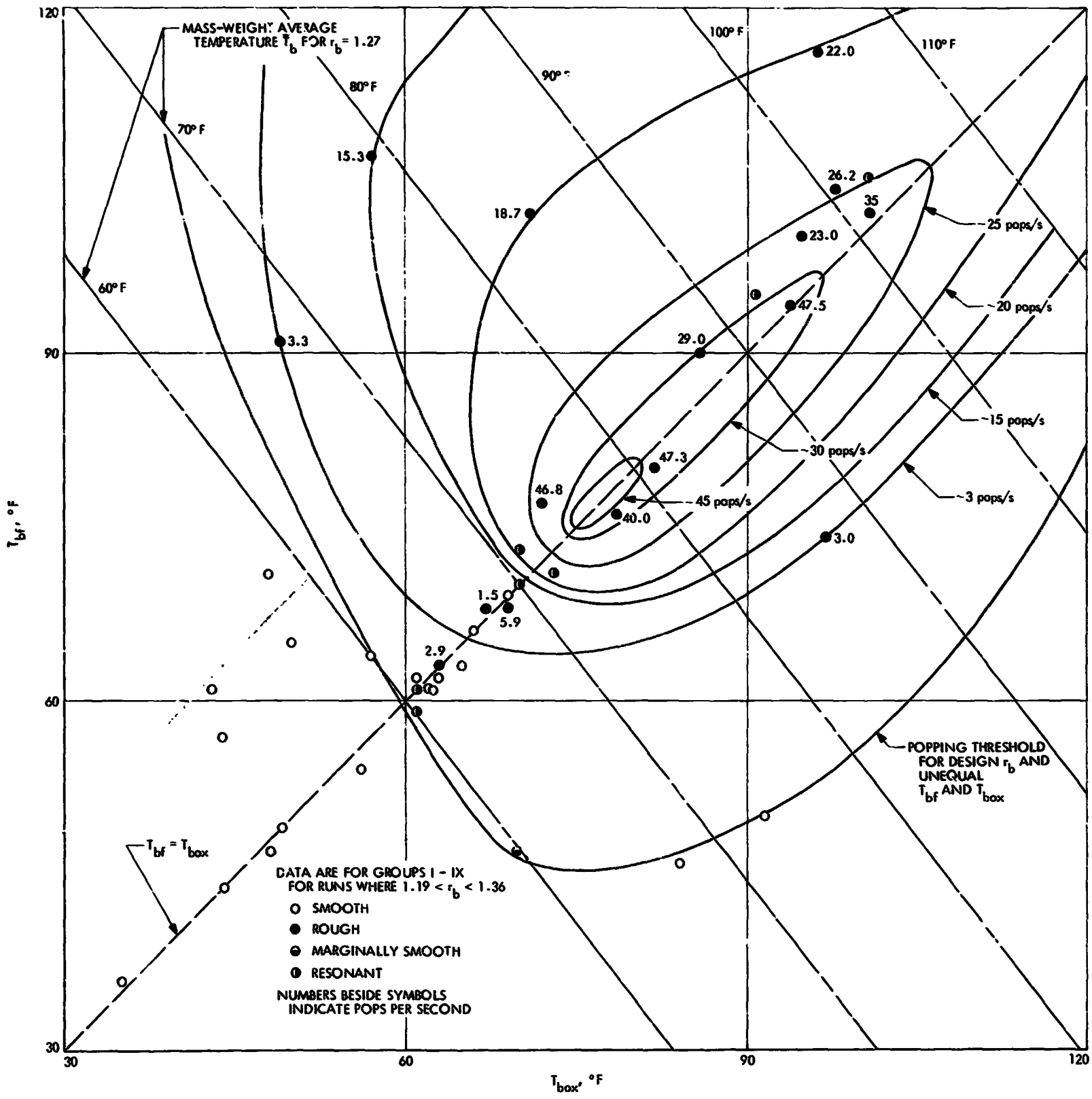

Fig. 20. Popping occurrence vs T_{bf} and T_{box} for r_b near 1.27, showing greater dependence of popping on fuel temperature

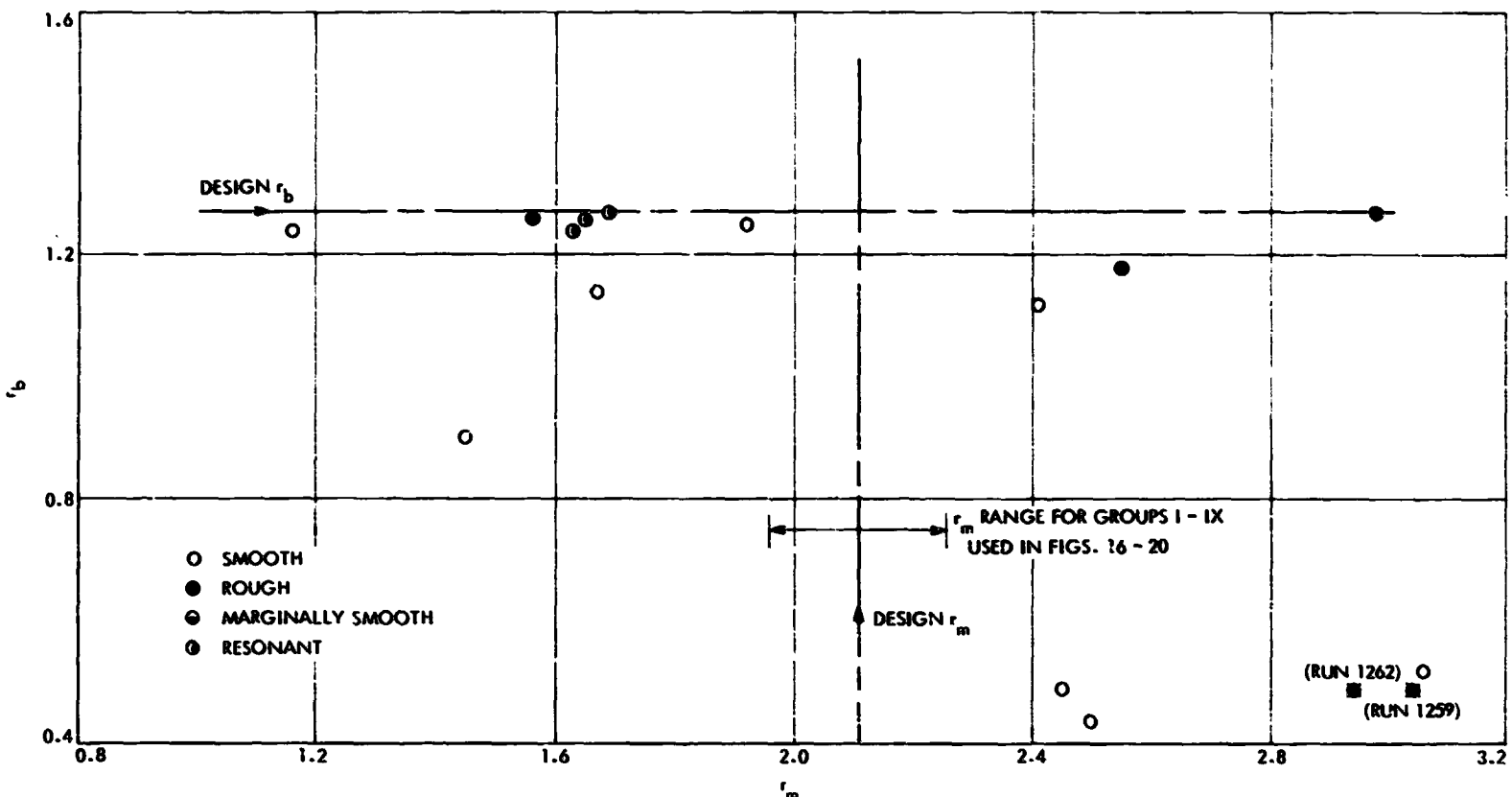

Fig. 21. Popping occurrence vs r_b and r_m for runs with simultaneous r_b and r_m variations, showing exceptions to dependency of popping on boundary flow conditions

Data from several firings with other off-design flow configurations were also obtained to further define operating conditions producing pops. The results from these firings are summarized separately in the paragraphs that follow.

1. Single boundary element separately controlled. This experiment was conducted to ascertain whether pops could be produced by a single boundary element. One element was arbitrarily chosen to have its mixture ratio and propellant temperature controlled separately from the remaining 23 boundary elements. These elements and the main elements were controlled in the normal manner. One firing was made with nominal design r_m and with the 23 boundary elements flowing at the nonpopping r_b of 0.44. The single element was supplied with 84°F propellants at a mixture ratio of 1.29—a condition well within the popping regime depicted in Fig. 19. Flow from the single element was initiated in the final 250 ms of a 2-s firing; two pops were produced within that period. No pops were produced during the earlier portion of the run.

2. Boundary flow only (main flow deleted). Pops were not observed during that period of the normal start sequence wherein boundary flows were established for 150 to 200 ms before commencement of the main flow (Section II-B). To verify this absence of pops when no main flow was present, a 2-s firing was conducted with boundary flow only. The r_b and $\bar{T}_b$ were well within the popping regime; no pops were detected during the entire firing.

3. Main flow only (boundary deleted). Several firings were conducted, with the boundary flow deleted, over a range of r_m and $\bar{T}_m$ conditions. These data are plotted in Fig. 23, which shows that no popping was ever produced for this operating configuration.

4. Boundary propellant substitutions. Several firings were conducted with single-propellant boundary flow (either 50/50 fuel or N_2O_4 oxidizer), and with bipropellant flow using N_2O_4–furfuryl alcohol (instead of 50/50 for the fuel). The normal main-flow propellants were retained.

For the single-propellant tests (Groups XII, XIII, and XIV), the two boundary manifolds were coupled together at their entrances and fed from a single source—either the fuel or oxidizer boundary feed system. Flow rates to the individual manifolds were not measured, but individual injector pressure drop data indicated that the measured total flow was essentially equally divided between the two manifolds. This produced a like-on-like impingement configuration, with nearly equal stream momenta.

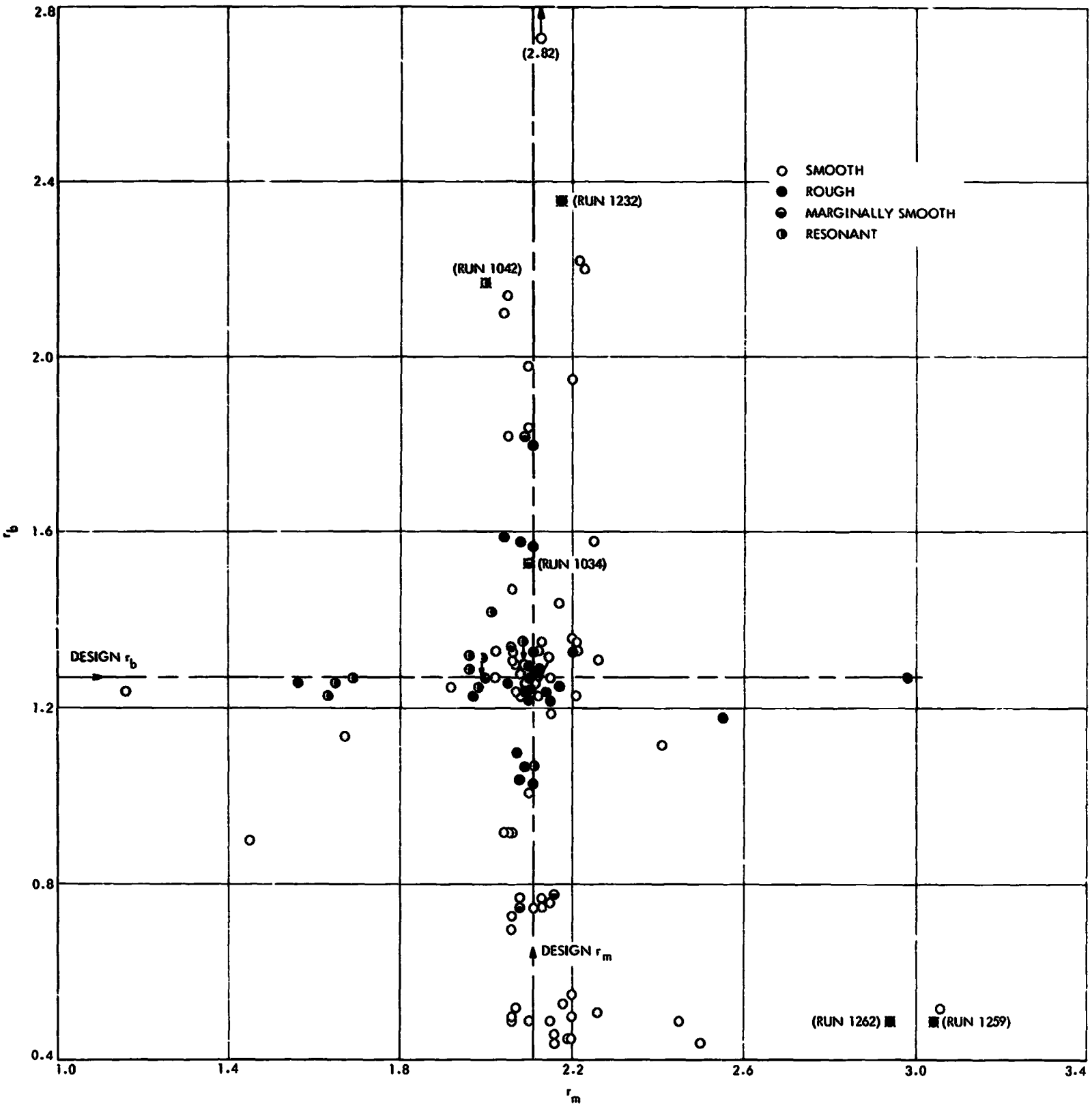

Fig. 22. Popping occurrence vs r_b and r_m for all runs, showing total exceptions to dependency of popping on boundary flow conditions

Table 6. Data for exceptions noted in Fig. 22

Run	Group	$\bar{T}_b$	$\bar{T}_m$	Remarks
1034	VI	51	46.5	Marginally smooth
1042	IV	68	64	Spontaneously resonant
1232	IX	68.5	56.5	Low popping rate
1259	IX-A	72.5	98	Low popping rate and amplitude
1262	IX-A	68.5	72	Low popping rate

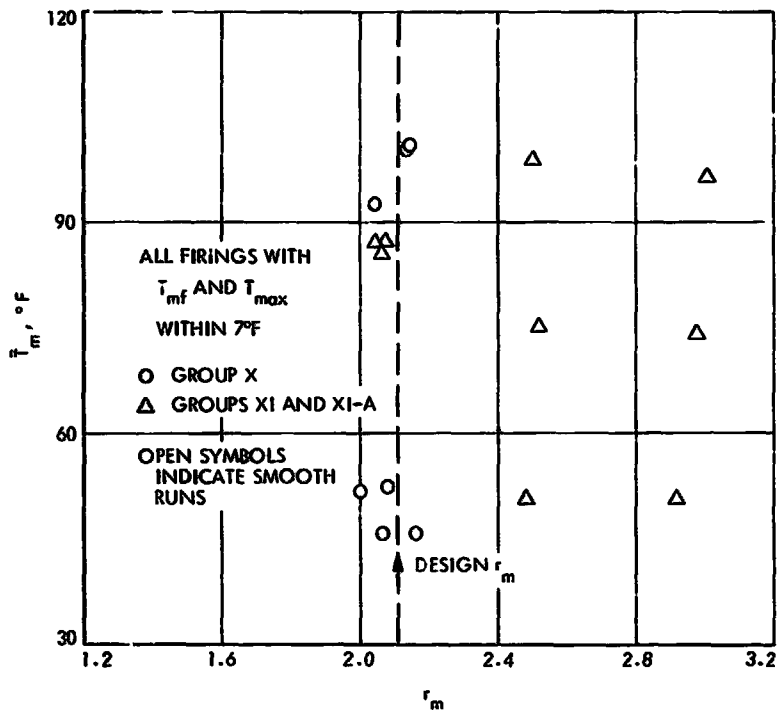

Fig. 23. Popping occurrence vs r_m and $\bar{T}_m$, showing absence of popping with no boundary flow

With the single-propellant oxidizer, no popping was observed during the three firings, as is indicated for the Group XIV runs (see Table 5), even though temperatures in the range of 70 to 77°F were used. Also, no popping was observed in three single-propellant fuel (50/50) runs with temperatures from 60 to 63°F (Group XII). However, when the fuel temperature was increased to 86°F, pops were produced at a rate of about 9.5 pops/s (run 1254, Group XIII). The boundary-mass fraction for this latter run appears to indicate a substantially higher boundary flow rate than it does for the cylindrical-engine runs of Group XII with which it is being compared; in fact, the flow rate is nearly the same value as that for run 1075. The large difference in Z is the result of the lower main flow rate of the annular engine (see Table 1).

In view of the concept of the stability of the impingement process that is discussed below, a final experiment with single-propellant boundary fuel was conducted with a restrictor inserted at the inlet to the outer boundary manifold to unbalance the momentum of the streams. Pressure-drop data indicated that the desired imbalance of ~2.75:1 (inner to outer stream) was achieved. This firing did not produce pops with a T_{bf} of 108°F.

Substitution of the furfuryl alcohol was accomplished by supplying the alcohol to the inner boundary manifold, which is normally the fuel manifold. Two firings were conducted (runs 1251 and 1252 of Group XV-A) nearly at the uniformity mixture ratio (nominally 1.13) for these propellants and the equal-diameter boundary elements. During run 1251, low-amplitude pops were present (~6.1 pops/s) throughout the first 1.7-s period of the 2-s run. At the end of this period, resonance was initiated spontaneously even though the annular engine was baffled and had previously demonstrated stability during many firings with bombs and substantial popping amplitudes. In the subsequent run, resonance was again spontaneously initiated after approximately 450 ms of the low-level popping. The loss of stability was a surprising result of the propellant substitution, and no attempt to explain it will be made here. The influence of the alcohol in reducing the severity of popping *per se* will be discussed below.

5. Elevated chamber pressure. A single firing (run 1255, Group XV-A) at 300-psia chamber pressure was made, as mentioned above. The injected flows were maintained near the design values with a $\bar{T}_b$ of 89.5°F (a popping condition for the 100-psia firings), but no pops were produced.

6. Summary of miscellaneous off-design firing results. Pops *were* produced with:

(1) A single boundary element (with main flow and with the remaining boundary elements at off-popping conditions).

(2) High-temperature, single-propellant boundary fuel (with main flow) if the like-on-like element was operated with nearly equal stream velocity.

(3) Furfuryl alcohol fuel (with N_2O_4 oxidizer) in the boundary (reduced pop amplitudes and rates).

Pops *were not* produced with:

(1) Main flow only.

(2) Boundary flow only.

(3) Single-propellant boundary *oxidizer* under any condition tested (with main flow).

(4) High-temperature, single-propellant boundary fuel (with main flow), if the like-on-like element was operated with nonidentical stream velocities.

(5) 300-psi chamber pressure.

IV. Discussion

In view of the results presented in the foregoing sections, it is evident that popping is the consequence of combustion-supported traveling waves originating from source disturbances, which (in the case of the engines studied herein) are associated with the boundary-injection system. Both a source disturbance and an appropriately reactive surrounding environment apparently are necessary to produce a pop.

Kovitz (see Ref. 6) has concluded that the reactive environment in the rocket chamber is indeed an appropriate one, especially in the region within a few inches of the injector in which high-temperature, *nearly complete* reactions abound. Although it is not clear how great a role the heterogeneous nature of this region plays in supporting disturbances in actual rocket combustors, other investigators (see Ref. 7) have concluded (from detonation-tube experiments) that combustion-supported, high-amplitude, high-velocity waves can be formed with relative ease in a combustible medium with either fuel sprays or fuel-wetted walls. In general, therefore, it is believed that high-performance, liquid rocket combustion systems always produce an appropriate environment to yield pops (given the initial source disturbances). Consequently, it is imperative to interpret the present results in terms of a relationship between engine-operating conditions (i.e., mixture ratio and propellant temperature) and an explicit popping source so that at least this source may be further understood and ultimately controlled.

A. Stagnation Dynamics of Impingement

It is beyond the scope of this report to present a formal analysis of the resultant flow field from a pair of impinging free jets. Instead, reference is made to an analysis[3] (Ref. 21) that discusses the important fact that the resultant flow can assume three topologically distinct configurations, depending upon the relative dynamic pressures of the two incoming streams.

[3]Suggested by Dr. D. F. Dipprey.

The three configurations depicted in Fig. 24 (adapted from Ref. 21) are for two-dimensional, inviscid, incompressible streams (sheets). If the ratio of stream dynamic pressures is arbitrarily defined as $p_{df}/p_{dox} = \rho_f V_f^2/\rho_{ox} V_{ox}^2$, where ρ and V are propellant density and stream velocity, respectively, then the configurations are identified in Fig. 24 as follows: (1) Fig. 24a for $p_{df}/p_{dox} < 1$, (2) Fig. 24b for $p_{df}/p_{dox} = 1$, and (3) Fig. 24c for $p_{df}/p_{dox} > 1$. The flow field for viscous, cylindrical streams of fluid possibly is not so straightforward, but physics requires that it exhibit the same gross feature: that only for equal dynamic pressures will both streams stagnate, and unequal dynamic pressures will produce only one stagnated stream.

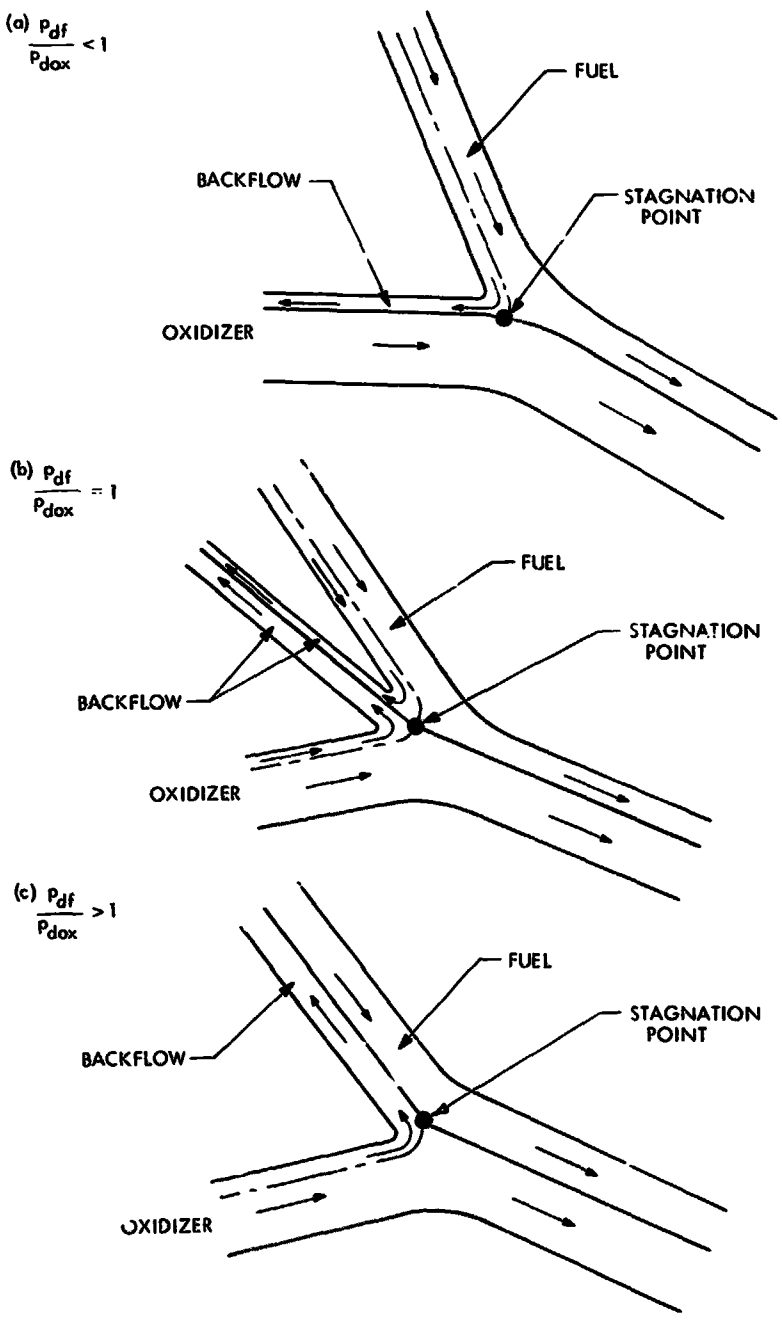

Fig. 24. Schematic representation of the impingement region for two-dimensional free liquid jets

One important characteristic of the flow field for each particular configuration is the production of "backflow" by a bifurcation of the stagnated stream(s). Conceptually, for a given doublet injector element, as the dynamic pressure ratio is varied from <1 through unity to >1, the resulting backflow will vary as depicted in Fig. 24. However, even if the pressure-ratio variation is continuous, the composition of the backflow will vary discontinuously as the pressure ratio passes through unity. Thus, operation of a doublet element near unity dynamic pressure ratio is evidently hydraulically unstable because, even for the best of flow systems, relative minor variations in flow (e.g., turbulent flow) or fluid density can occur that may temporarily shift the stagnation–streamline pressure ratio from one side of unity to the other.

The production of backflow causes the effluent mixture ratio (downstream from the impingement point) to be different from the overall mixture ratio of the incoming streams. Although the backflow is eventually consumed (in the case of reactive fluids), it cannot be considered as taking part in the primary mixing processes. For *two-dimensional inviscid streams*, it can be shown from mass and momentum balances (see Ref. 21) that the "split ratio" X of the bifurcated stream (for the case $p_{df}/p_{dox} \neq 1$) is:

$$X = \frac{(1 + \Gamma)(1 + \cos\alpha)}{2 + \Gamma(1 + \cos\alpha)}$$

where X is the ratio of the effluent-to-input mass flow rate of the bifurcated stream, Γ is the ratio of the oxidizer-to-fuel momentum fluxes, and α is the included impingement angle between the two incoming streams.

From these relationships, it can be shown that the mixture ratio of the effluent flow r_2 can be related to the overall input mixture ratio r_1 by $r_2 = Xr_1$ for $p_{df}/p_{dox} > 1$, and $r_2 = r_1/X$ for $p_{df}/p_{dox} < 1$.

If it is assumed that the cylindrical-stream impingement of the boundary elements follows this two-dimensional backflow relationship, Fig. 25 shows how, for this element, the output mixture ratio r_{b2} might vary with input mixture ratio r_{b1} (equal to r_b), for a nominal propellant–density ratio ρ_{ox}/ρ_f of 1.613 at a temperature of 40°F. Dynamic pressure ratio vs r_b is also shown because dynamic pressure ratio can be expressed as:

$$\frac{p_{df}}{p_{dox}} = \frac{\rho_f V_f^2}{\rho_{ox} V_{ox}^2} = \frac{\rho_f \dot{m}_f^2 d_{ox}^4 \rho_{ox}^2}{\rho_{ox} \dot{m}_{ox}^2 d_f^4 \rho_f^2} = \frac{1}{r_b^2} \frac{\rho_{ox}}{\rho_f} \left(\frac{d_{ox}}{d_f}\right)^4$$

where $\dot{m}_f$ and $\dot{m}_{ox}$ are the input mass flow rates of an element of the boundary system.

It should be noted that the design mixture ratio of 1.27 corresponds to $p_{df}/p_{dox} = 1$ for the propellant temperature used in this illustration. However, because the density ratio varies only slightly with temperature, operation at $r_b = 1.27$ will always produce a pressure ratio near unity for this element and N_2O_4–50/50 propellants.

In the case of the injector RC-1 boundary system, 24 elements are fed from common manifolds, and the measured r_b for any particular firing is the mean value for the multiple elements. Not all elements (perhaps none) will operate at the measured value, depending upon the flow distribution from the manifolds. Thus, a more or less random distribution of mixture ratio (hence pressure ratio) around the mean value would be expected for the individual elements. In poorly controlled manifold schemes, the mean value might not even be representative of the element flow. In any case, the net effect of multiple elements is to smear the effects of single-element impingement processes over a broader range of mean operating values.

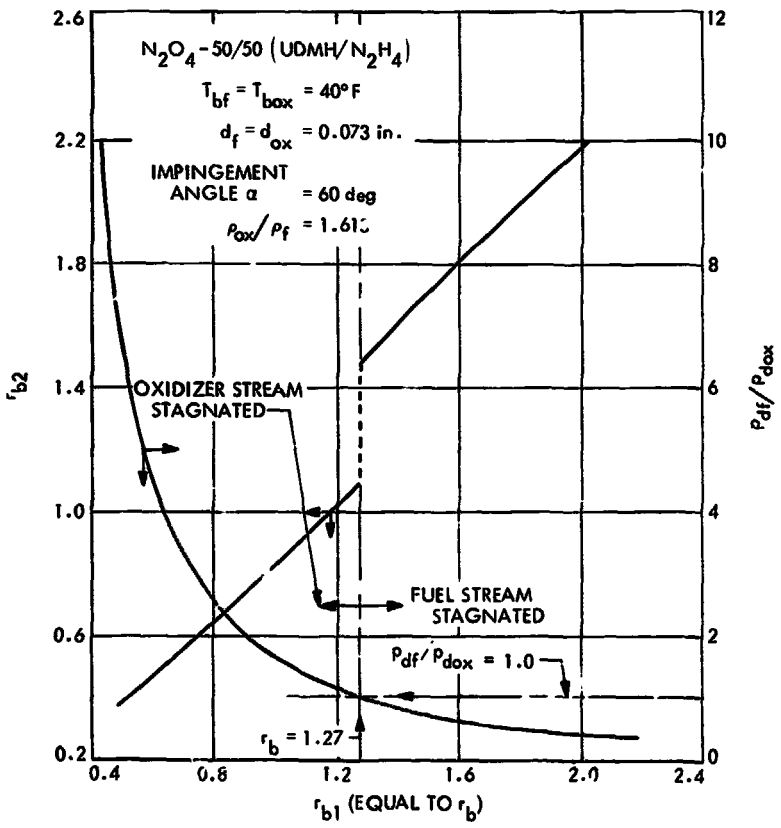

Fig. 25. Computed output mixture ratio and dynamic pressure ratio vs input mixture ratio for boundary element, based on two-dimensional inviscid analysis

B. Hypergolic Reactivity in Stagnation Region

Recent studies of hypergolic stream impingement (see Refs. 11–13) have shown that heat release and gas evolution from rapid reactions in the impingement region can, in certain cases, modify the mixing and atomization processes observed for nonreactive fluids. These so-called stream-separation effects are not yet fully understood; however, three interrelated parameters have been identified that appear to be important: (1) propellant temperature, (2) impingement contact time, and (3) total pressure at the impingement interface.[4] This interrelationship appears to involve the level of reactivity of the particular propellants being considered.

The current concept of the stream-separation phenomenon is that there is a finite time of intimate contact of the reactants at the impingement interface. If the reactivity of the fluids is vigorous enough, sufficient gas products (or reactant vapors) will be evolved during the contact time to effectively separate the streams and prevent gross liquid mixing. However, if the reactions are sufficiently slow relative to the contact time, the mixing and atomization of the streams follow essentially the same course of events for nonreactive impingement. Because reactant temperature has a large effect on reaction rate, it is not surprising that separation can be a function of both temperature and contact time for a given propellant combination.

A complication to this concept is the influence of total interface pressure. Theoretical models of stream separation have postulated three mechanisms (see Ref. 13):

(1) Local boiling of propellants caused by heat released by liquid-phase reaction.

(2) Gas evolution caused by gaseous products of liquid-phase reactions.

(3) Formation of a gas film between jets caused by gas-phase reaction.

Typical analytical results obtained from these models are illustrated in Fig. 26. The pressure is predicted to have a primary influence on the occurrence of separation for all three mechanisms; however, its effect in mechanism (1) is opposite to its effect in mechanisms (2) and (3). That is, for a given contact time, increasing pressure suppresses separation for evaporative mechanism (1), whereas it enhances separation for the other two mechanisms. Therefore, if all of these mechanisms are present, the effect of pressure depends upon the mechanism that is controlling.

Even the dependency of separation on propellant temperature is not universal for the three models because, for mechanism (3), such a small temperature dependence is predicted that it is too small even to show on Fig. 26.

Insufficient experimental data have been obtained to evaluate these models adequately or to establish the possible application of each, but temperature, pressure, and contact time appear to be the dominant parameters for a given propellant combination.

Perhaps the greatest deficiency in modeling the separation phenomena so far is the definition of contact time. A rigorous analytical definition of this parameter is almost impossible because of the complex nature of the three-dimensional hydrodynamic flow field encountered in practical injector-element geometries; therefore, for analytical simplification, contact time was originally defined (see Ref. 12) for a pair of axially symmetric, 180-deg opposed, inviscid streams of equal velocity for which the impingement could be considered as if it occurred normal to a flat plate. In this case, the characteristic *average residence time* of a particle along the impingement interface was shown to be approximately equal to d/V, where d and V are jet diameter and velocity, respectively. This definition has been used subsequently in all published work on stream separation.

The foregoing models of stream separation evoke the condition of equal stream dynamic pressures. It is believed that the fact that only an average residence time was considered overlooks the possibility that a small kernel of both reactants in the immediate vicinity of the impingement point may indeed be stagnant, and hence have an infinite residence time. For practical elements (with turbulence and other nonsteadiness), this time is undoubtedly not infinite, but merely much greater than the average residence time indicated by d/V. In fact, d/V may be more nearly the correct contact time for streams with unequal dynamic pressures, in which (as discussed in Section IV-A) only the stream of lower dynamic pressure is stagnated. In this case, contact time might be defined as proportional to the diameter of the stagnated jet divided by the velocity of the unstagnated jet. The point is that again the condition of equal dynamic pressures appears to present an essentially discontinuous effect on the impingement processes.

[4]Total interface pressure = chamber pressure + dynamic pressure of stagnated jet.

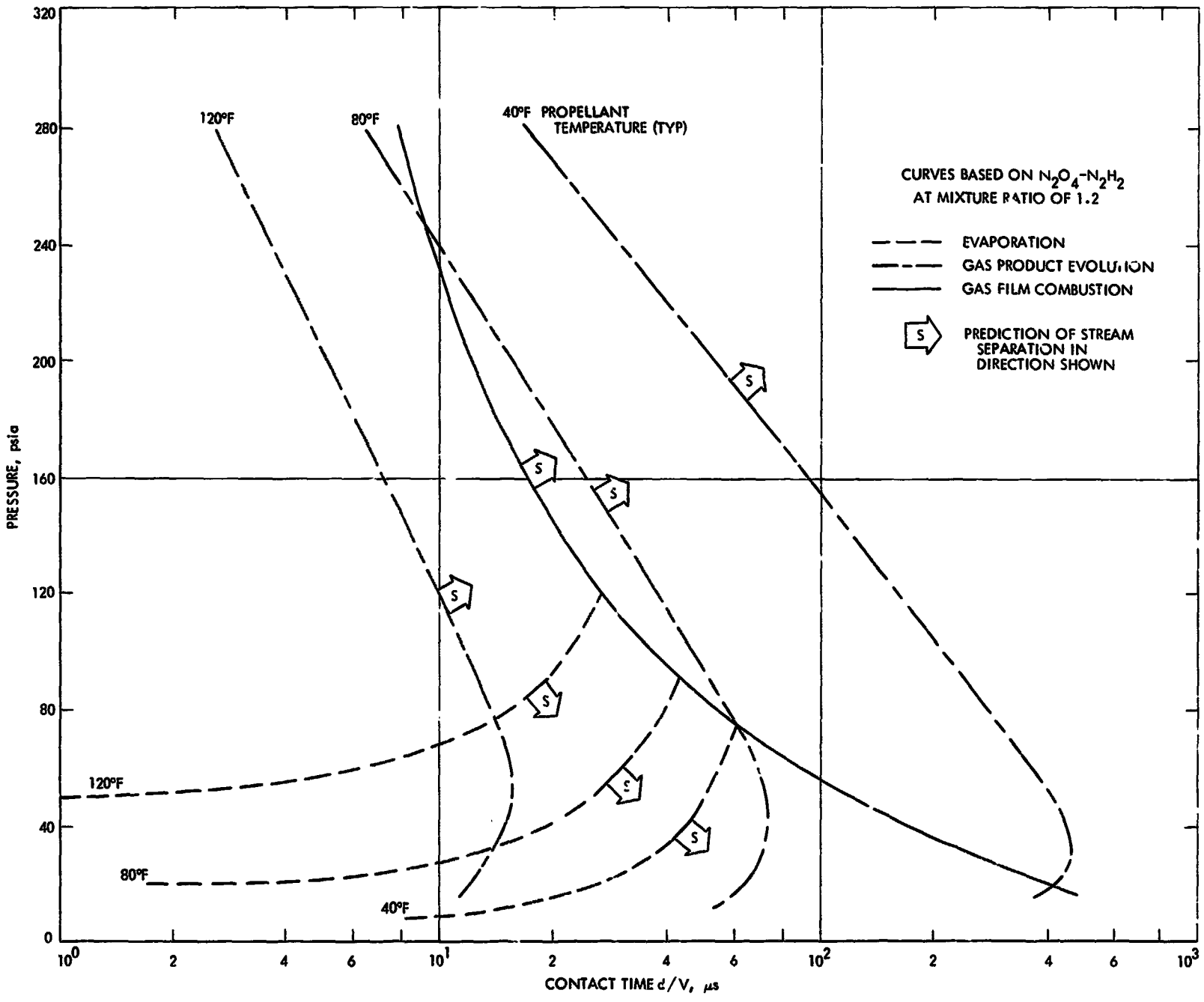

Fig. 26. Typical results of stream-separation models (after Houseman, Ref. 13)

This is illustrated in Fig. 27, which shows contact time vs $(1 + p_{df}/p_{dox})^{-1}$ for the boundary elements of the RC-1 injector. Contact time in this case is defined as the diameter of the boundary orifice (0.073 in.) divided by the velocity of the unstagnated stream (N_2O_4–50/50 propellants were assumed). An average contact time of approximately 80 μs is indicated for unity p_{df}/p_{dox}, but that contact time for this condition is actually undefined for the reasons previously given. Conceptually, the contact time in the vicinity of unity dynamic pressure ratio follows the trend shown by the dashed curve, where its faired-in nature reflects the fact that the unstagnated stream decelerates as it *approaches* the stagnation condition; hence, contact time probably increases with the trend shown.

C. Correlation of Popping Occurrence With Dynamic Pressure Ratio

To apply the foregoing concepts of chemically reactive impingement dynamics to the question of pop sources, it is suggested that a small kernel of reactant(s) may be essentially stagnant at the impingement point, but the composition of this kernel may be either all one reactant or both, depending on the relative stream dynamic pressures. Thus, for $p_{df}/p_{dox} \ll 1$ (see Fig. 27), the fuel stream is stagnated, with the oxidizer sweeping past the stagnated kernel of fuel, and *vice versa*. In such a case, the contact time may be relatively short compared to the case where both streams are nearly stagnated (or alternately stagnated), when the stagnant kernel may be composed of both reactants with a long time to react. It is envisioned that this latter situation could produce a small "explosion" that could be the source disturbance for a pop, whereas the former cases may produce some degree of stream separation only, the actual production of either the pop-source disturbance or stream separation still being a function of chemical reactivity, contact time, and total pressure at the interface.

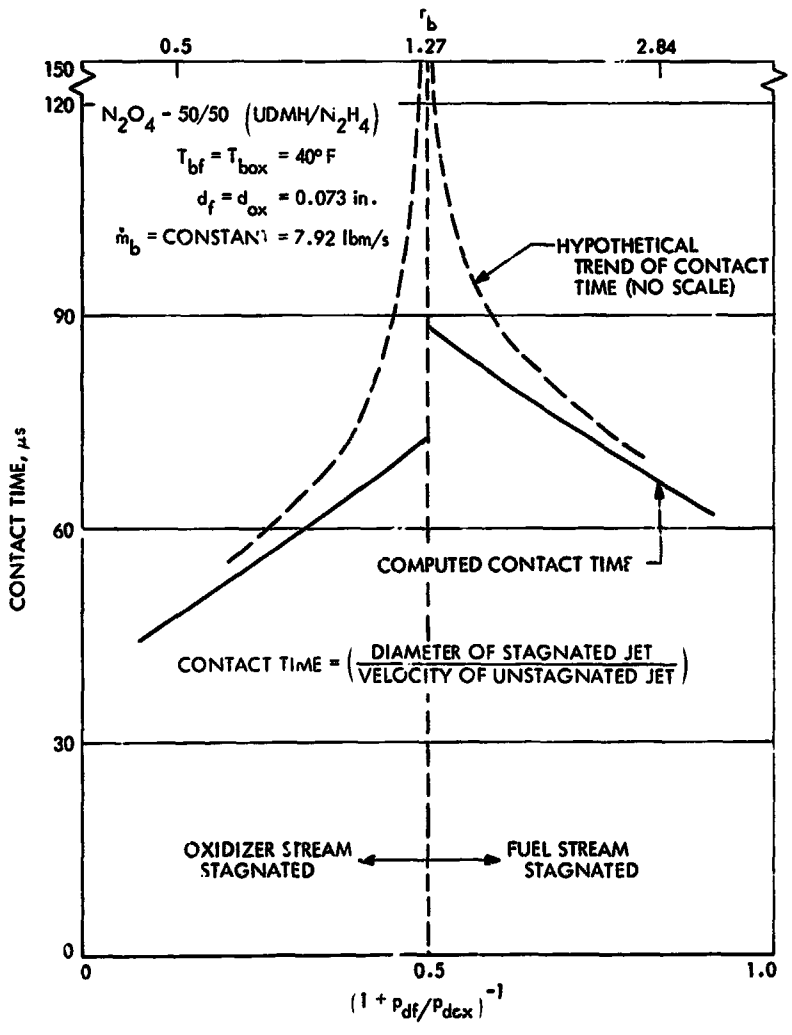

Fig. 27. Contact time vs dynamic pressure ratio parameter $(1 + p_{df}/p_{dox})^{-1}$

The probability that the entire impingement configuration is temporarily disrupted by the source disturbance (see Refs. 4 and 5), requiring some time to return to its initial configuration before repeating the explosive event, could lead to the randomness of popping in a rough run. The presence of multiple elements in the injector would tend to accentuate the randomness and (as previously discussed) broaden the mean operating range over which pops are produced.

The engine data illustrated in Fig. 19 are presented in terms of dynamic pressure ratio in Fig. 28. In this figure, the data are not identified as to group (see Table 5). The popping-rate contour lines show how popping occurrence is maximized around $p_{df}/p_{dox} = 1$ at $75°F < \overline{T}_b < 80°F$, although popping occurred over a fairly broad range of pressure ratio, as might be expected for the multiple elements.

The fact that the occurrence of popping was a function of pressure ratio and propellant temperature is believed to be consistent with the arguments discussed above regarding the stability of the impingement process, the increase in contact time at unity pressure ratio,[5] and increased reactivity with increasing temperature. However, the tendency for popping rate to decrease for propellant temperatures above 80°F is difficult to rationalize at this time. But it is possible that the generation of the explosion-like pop source is associated with some range of

[5]Interestingly, almost all reported results on single-element stream separation and popping investigations are for equal dynamic pressure streams.

intermediate impingement cone[illegible] between the inception of stream separation and [illegible] development. Other investigators have also observed [illegible] tendency,* which they have attributed to a requirement for some degree of liquid-phase mixing to have occurred before the disturbance can be created. In the absence of more definitive information, this is believed to be a plausible explanation for the present results. For near-unity dynamic pressure ratio, temperatures below ~60°F did not allow appreciable gas or vapor evolution within the impingement region, whereas temperatures in the range of 75 to 80°F apparently provided an optimum combination of mixing and gas evolution (albeit sporadically). Finally, at temperatures above 80°F, still greater gas (or vapor) evolution reduced liquid-phase mixing and, therefore reduced the random generation of pop-source disturbances.

The contention throughout this discussion that the source of an individual pop is produced by a single element is borne out by the pop-location data presented in Section III-A, and is confirmed by the separately controlled, single-element experiment described in Section III-B. The popping-rate data obtained for the composite injector are the result of many elements producing pop sources. The fact that a maximum popping rate was observed at the *mean* operating condition $p_{inj}/p_{dot} = 1$ is, in one sense, an indication of the relatively good flow distribution of the RC-1 boundary manifold; that is, a large number of the elements were indeed flowing at the mean condition.

The fact that popping was eliminated in the one firing where chamber pressure was increased from 100 to 300 psia indicates that the reactive-impingement pop-source mechanism is suppressed by increased combustion pressure. This is reminiscent of the effect of increased pressure in suppressing the boiling mechanism of vapor evolution (Section IV-B). However, increased pressure is also predicted to enhance the gas product and gas film combustion mechanisms of stream separation; therefore, the observed suppression effect of higher pressure remains unexplained at this time. Nevertheless, the effect of suppression by increased combustion pressure should not be ignored; it is similar to the observations of Houseman (see Ref. 13) for N_2O_4–N_2H_4 propellants in a small single-element (same element size as the present boundary element) research combustor. He reported a marked decrease in roughness (albeit not clearly pops) for chamber pressures above 150 psia.

The effect of the level of reactivity on the production of pop sources was cursorily examined in the experiments that used furfuryl alcohol as fuel in the boundary system. The N_2O_4–furfuryl alcohol combination is thought to have a reaction rate lower by an order of magnitude than the N_2O_4–50/50 combination; hence, according to the reactive-impingement-dynamics concept of pop sources, a substantial change in popping characteristics should be observed with furfuryl alcohol. Qualitatively, a change was observed: greatly reduced pop amplitudes and rates were exhibited for the two firings that were conducted.

When chemical reactivity in the impingement region was eliminated by the use of like-on-like boundary injection, pops were produced only when fuel was used at an elevated temperature. It is not believed that this refutes previous arguments concerning the reactivity of hypergolic impingement; rather, it is believed that this indicates the critical influence of dynamic pressure ratio on the stability of the impingement process. Even if there is no chemical reactivity, the hydrodynamic properties of impingement shown in Fig. 24 still apply, and the efflux from the impingement for unity dynamic pressure ratio is still inherently unsteady. To couple this unsteadiness (as a pop source) with the combustion environment (recalling that a pop is the result of a combustion-supported wave induced by a source disturbance), it is necessary to note that the main injection system for these engines is known to produce an oxidizer-rich environment around the outer periphery of the main element-pattern (see Ref. 8), presumably because of stream separation from these large-scale elements. When oxidizer like-on-like boundary injection was used, the unsteadiness in the boundary sprays did not produce pops because the oxidizer boundary was essentially not reactive with the already oxidizer-rich surrounding environment. However, when high-temperature fuel was used in the boundary, substantial reactivity was possible. Fuel-source perturbations were then effective in generating pressure waves that were further amplified as they progressed across the chamber. This is evidently not as effective a source generator as bipropellant impingement at unity pressure ratio because a lower rate of popping was produced (9.5 pops/s vs ~45 pops/s). Even this source was eliminated by operating the like-on-like fuel streams at unequal dynamic pressures. Perhaps one reason for this reduced popping tendency is the probability that the effective pop source occurs farther downstream in the combustor, and hence the source disturbances are less apt to couple with the early reaction zone of the chamber.

*Private communication with B. P. Breen and B. H. Lawver.

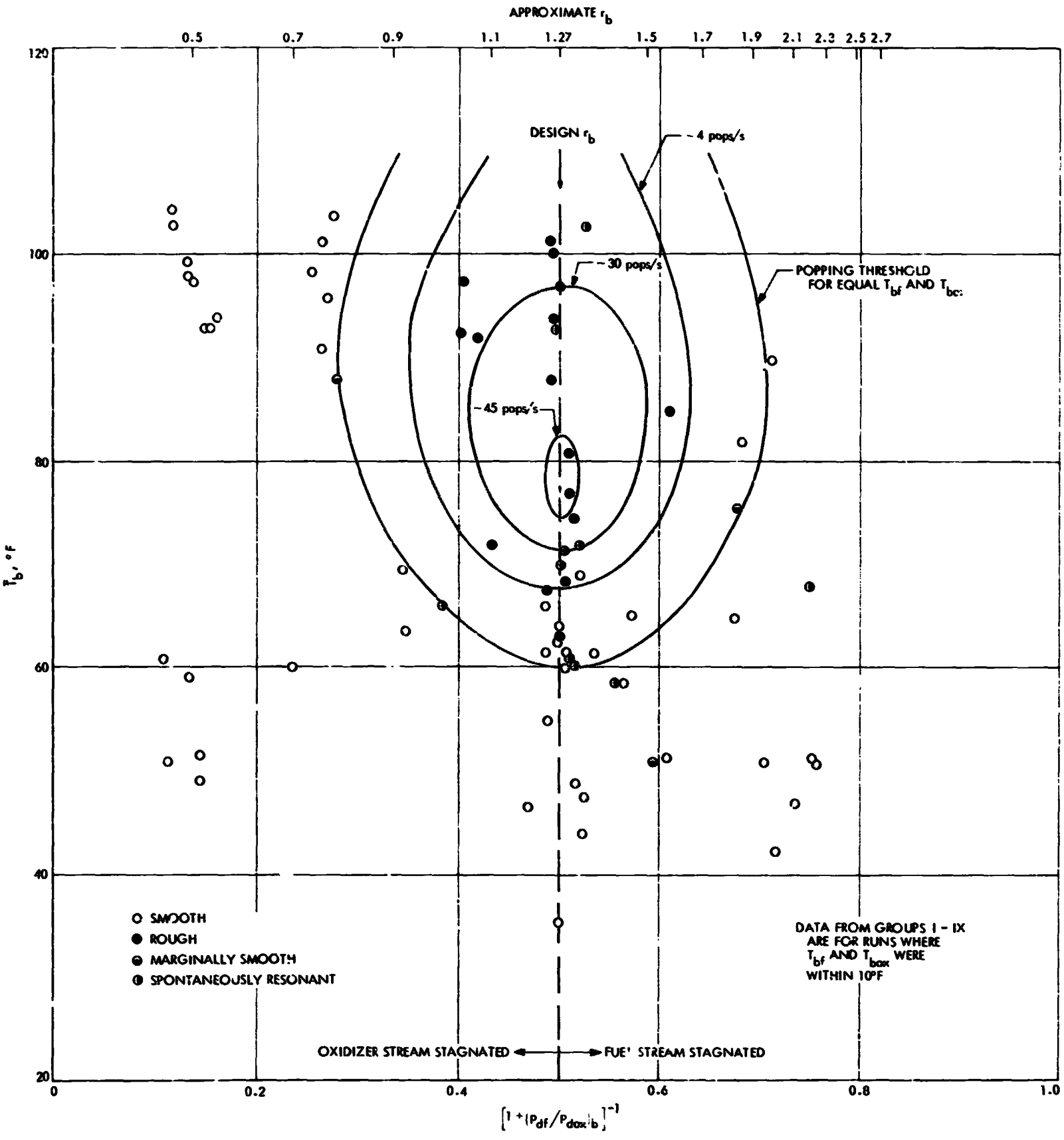

Fig. 28. Popping occurrence vs $\bar{T}_b$ and dynamic pressure ratio parameter $(1 + p_{df}/p_{dox})^{-1}$

For equal-diameter doublet streams, the mixing-uniformity-criterion ratio (see Ref. 15) and the momentum ratio for the streams are numerically equal to the dynamic pressure ratio. Hence, the pressure-ratio correlation reported herein could be interpreted as a correlation with any of the three ratios. In a cursory attempt to resolve this ambiguity, an examination was made of the data from firings that had used only the main elements. No popping was exhibited for any of the firings, even though the data (shown as $\overline{T}_m$ vs r_m in Fig. 23) covered a dynamic pressure ratio range of 0.68 to 1.57, with temperatures from 50 to 100°F. This range of pressure ratios includes the flow condition for unity-mixing-criterion ratio ($p_{if}/p_{dox} = 1.4$ for the unequal-diameter main-element streams), but only approaches the condition for equal-stream momenta ($p_{df}/p_{dox} = 1.97$); therefore, the ambiguity was not clearly resolved by the existing data.

However, the main-flow-only results are an indication that these main elements may never produce pops under any reasonable flow and temperature conditions (with N_2O_4-50/50 propellants) because of the large scale of the elements, which yield calculated contact times of approximately 130 μs. As already mentioned, the main elements exhibit considerable stream separation: perhaps this is sufficiently well developed to preclude adequate liquid-phase mixing in the impingement region for pop-source production. This high degree of stream separation may also overwhelm the inherent hydrodynamic unsteadiness for unity pressure ratio. Although it is not rigorously proven, a further criterion for suppressing popping tendencies may be the use of relatively large-scale elements. The high performance of the cylindrical engine (see Ref. 8) has shown that stream separation can be compensated for by the judicial use of secondary mixing.

V. Conclusions

A nontrivial source of popping in a liquid rocket engine is unsteady impingement processes related to stagnation dynamics and to rapid hypergolic reactions in the stagnated impingement region. In this sense, the production of pop sources is a regime of reactive stream-separation phenomena; however, the hydraulic unsteadiness associated with impingement of equal-dynamic pressure nonreactive streams can also act as a pop source. Therefore, the condition of equal dynamic pressure maximizes the tendency to produce combustion disturbances, regardless of stream reactivity.

The sources themselves are not the high-amplitude chamber pressure disturbances detected as pops because the latter are the result of amplification of the source waves through detonation-like processes. Once produced, a pop is extremely effective in precipitating combustion resonance, and highly effective attenuating devices (such as baffles) are required to stabilize the engine. Thus, to provide the highest margin of stability, the pop sources must be eliminated.

It is concluded, therefore, that control over the production of impingement-related sources lies within the control of the injection scheme itself, and that the first step in such control is to require that no impinging element be allowed to operate at the condition of equal stream dynamic pressures.

Nomenclature

c average propagation velocity of overall disturbance from pop-location analysis

c^* measured characteristic exhaust velocity

c^*_{th} theoretical equilibrium characteristic exhaust velocity

D orifice diameter

d jet diameter

$\mathcal{F}$ nominal propellant mass flux through chamber

L orifice length

$\dot{m}$ mass flow rate

p_c static chamber pressure

$p_{c\,rms}$ root mean square of pressure-amplitude variations caused by combustion noise

p_d jet dynamic pressure $\rho V^2/2$

r overall mixture ratio $\dot{m}_{ox}/\dot{m}_f$

r_b boundary mixture ratio

r_m main mixture ratio

T propellant temperature

$\bar{T}$ mass-weighted average propellant temperature

t time

V jet axial velocity

Z mass fraction ratio of boundary flow rate to total flow rate

η_c combustion efficiency 100 (c^*/c^*_{th})

ρ propellant liquid density

Subscripts

b boundary injection system

f fuel

m main injection system

ox oxidizer

t total flow rate

1 input value of mixture ratio

2 effluent mixture ratio of mixed flow

References

1. Hefner, R. J., "Review of Combustion Stability Development with Storable Propellants," *J. Spacecraft Rockets*, Vol. 3, No. 7, pp. 1046–1051, July 1966.

2. Valentine, R. S., Rossi, F. S., and Kromrey, R. V., "Fluid Dynamic Effects on Apollo Engine Pressure Spikes," *J. Spacecraft Rockets*, Vol. 5, No. 1, pp. 31–35, Jan. 1968.

3. Weisse, R. R., Chew, T. J. C., and Klopotek, R. D., "A Combustion Stability Evaluation of Various Hydrazine and Hydrazine Blend Fuels (U)," in *Bulletin of the Seventh Liquid Propulsion Symposium*, CPIA Publication 72, Vol. I, pp. 343–384, Aug. 1965 (Confidential).

4. Mills, T. R., et al., *Transients Influencing Rocket Engine Ignition and Popping*, NAS7-467, Interim Report SN-95D. Dynamic Science, A Division of Marshall Industries, Monrovia, Calif., Apr. 30, 1968.

5. Campbell D. T., et al., *Reactive Stream Separation Photography*, NAS7-720, Interim Report R-8110. Rocketdyne, A Division of North American Rockwell, Canoga Park, Calif., Jan. 10, 1970.

6. Kovitz, A. A., *Large Amplitude Resonant Combustion in Liquid Engine Chambers: Some Aspects of Initiation*, Technical Report 32-1377. Jet Propulsion Laboratory, Pasadena, Calif., Nov. 15, 1969.

7. Dabora, E. K., Ragland, K. W., and Nicholls, J. A., "A Study of Heterogeneous Detonations," *Astronaut. Acta*, Vol. 12, No. 1, pp. 9–16, 1966.

8. Clayton, R. M., *The Influence of Several Near-Wall Injection Conditions on the Combustion Performance of a Liquid Rocket Engine*, Technical Report 32-1283. Jet Propulsion Laboratory, Pasadena, Calif., Sept. 15, 1968.

9. Clayton, R. M., "Resonant Combustion," in *Supporting Research and Advanced Development*, Space Programs Summary 37-49, Vol. III, pp. 223–236. Jet Propulsion Laboratory, Pasadena, Calif., Feb. 28, 1968.

10. Clayton, R. M., "Resonant Combustion," in *Supporting Research and Advanced Development*, Space Programs Summary 37-55, Vol. III, pp. 245–257. Jet Propulsion Laboratory, Pasadena, Calif., Feb. 28, 1969.

11. Lawver, B. R., and Breen, R. P., *Hypergolic Stream Impingement Phenomena —Nitrogen Tetroxide/Hydrazine*, NASA CR 72444. Dynamic Science, A Division of Marshall Industries, Monrovia, Calif., Oct. 1968.

12. Kushida, R., and Houseman, J., *Criteria for Separation of Impinging Streams of Hypergolic Propellants*, Technical Memorandum 33-395. Jet Propulsion Laboratory, Pasadena, Calif., July 15, 1968. (Also presented at Western Section Combustion Institute, Paper WSCI-67-38, Seattle, Wash., Oct. 30–31, 1967.)

13. Houseman, J., "Combustion Effects in Sprays," in *Supporting Research and Advanced Development*, Space Programs Summary 37-54, Vol. III, pp. 128–132. Jet Propulsion Laboratory, Pasadena, Calif., Dec. 31, 1968. (Also published in *Expanded Abstracts and Slides of the Fifth ICRPG Combustion Conference*, CPIA Publication 183, pp. 255–261, Dec. 1968.)

References (contd)

14. Clayton, R. M., "Resonant Combustion," in *Supporting Research and Advanced Development*, Space Programs Summary 37-56, Vol. III pp. 204–212. Jet Propulsion Laboratory, Pasadena, Calif., Apr. 30, 1969.

15. Rupe, J. H., *An Experimental Correlation of the Nonreactive Properties of Injection Schemes and Combustion Effects in a Liquid-Propellant Rocket Engine: Part I. The Application of Nonreactive-Spray Properties to Rocket Motor Injector Design*, Technical Report 32-255. Jet Propulsion Laboratory, Pasadena, Calif., July 15, 1965.

16. Clayton, R. M., Rupe, J. H., and Gerbracht, F. G., *An Experimental Correlation of the Nonreactive Properties of Injection Schemes and Combustion Effects in a Liquid Propellant Rocket Engine: Part II. Instrumentation, Experimental Apparatus, and Experimental Techniques*, Technical Report 32-255. Jet Propulsion Laboratory, Pasadena, Calif., May 15, 1967.

17. Clayton, R. M., and Rupe, J. H., *An Experimental Correlation of the Nonreactive Properties of Injection Schemes and Combustion Effects in a Liquid Propellant Rocket Engine: Part VI. The Relation Between the Starting Transient and Injection Hydraulics*, Technical Report 32-255. Jet Propulsion Laboratory, Pasadena, Calif., Oct. 29, 1965.

18. Clayton, R. M., and Rogero, R. S., *Experimental Measurements on a Rotating Detonation-Like Wave Observed During Liquid Rocket Resonant Combustion*, Technical Report 32-788. Jet Propulsion Laboratory, Pasadena, Calif., Aug. 15, 1965.

19. Kushida, R., "Resonant Combustion: Location of the Initial Disturbance in Spontaneously Resonant Rocket Engines," in *Supporting Research and Advanced Development*, Space Programs Summary 37-58, Vol. III, pp. 225–228. Jet Propulsion Laboratory, Pasadena, Calif., Aug. 31, 1969.

20. Bonnell, J. M., *An Investigation of Spherical Blast Waves and Detonation Waves in a Rocket Combustion Chamber*, Technical Report 32-1286. Jet Propulsion Laboratory, Pasadena, Calif., Aug. 15, 1968.

21. Rupe, J. H., et al., "The Stability Criterion for Impinging Jets and its Impact on Combustion," in *Expanded Abstracts and Slides of the Sixth ICRPG Combustion Conference, Chicago, Ill., September 9–11, 1969*. CPIA Publication 192, Vol. 1, pp. 1–11, Dec. 1969.